

Technical Report
1065

Theoretical Effects of Array Mutual Coupling on Clutter Cancellation in Displaced Phase Center Antennas

A.J. Fenn
E.J. Kelly

5 September 2000

Lincoln Laboratory

MASSACHUSETTS INSTITUTE OF TECHNOLOGY

LEXINGTON, MASSACHUSETTS



Prepared for the Department of the Air Force under Contract F19628-00-C-0002.

Approved for public release; distribution is unlimited.

THIS DOCUMENT IS UNCLASSIFIED

20000920 067

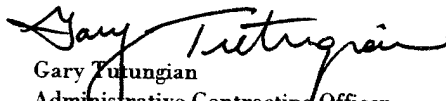
This report is based on studies performed at Lincoln Laboratory, a center for research operated by Massachusetts Institute of Technology. The work was sponsored by the Air Force under Contract F19628-00-C-0002.

This report may be reproduced to satisfy needs of U.S. Government agencies.

The ESC Public Affairs Office has reviewed this report, and it is releasable to the National Technical Information Service, where it will be available to the general public, including foreign nationals.

This technical report has been reviewed and is approved for publication.

FOR THE COMMANDER


Gary Tutungian
Administrative Contracting Officer
Plans and Programs Directorate
Contracted Support Management

DESTRUCTION NOTICE

Permission is given to destroy this document when it is no longer needed, by any method that will prevent disclosure of contents or reconstruction of the document.

MASSACHUSETTS INSTITUTE OF TECHNOLOGY
LINCOLN LABORATORY

**THEORETICAL EFFECTS OF ARRAY MUTUAL
COUPLING ON CLUTTER CANCELLATION IN
DISPLACED PHASE CENTER ANTENNAS**

*A.J. FENN
E.J. KELLY
Group 108*

TECHNICAL REPORT 1065

5 SEPTEMBER 2000

Approved for public release; distribution is unlimited.

ABSTRACT

Large phased array antenna systems are being considered for space-based radar (SBR) applications. One particular moving target indicator (MTI) radar system concept which looks promising uses the displaced phase center antenna (DPCA) implementation to cancel background clutter. Ignoring signal generation/processing issues, the ability to cancel clutter rests primarily on the DPCA array forming two (or more) displaced phase center radiation patterns having identical main beam characteristics. In an ideal array with no mutual coupling and no hardware errors, a DPCA array would have identical main beams. However, in a practical array, mutual coupling between the array elements will cause the displaced phase center antenna main beam shapes to become amplitude and phase mismatched. Thus, clutter can only be partially cancelled. It is desirable to quantify the effects of mutual coupling on DPCA performance.

The method of moments is used to model finite arrays of thin-wire antennas over an infinite ground plane. In this way, array mutual coupling and array edge effects are included in a numerical simulation of a DPCA phased array. Both sub-scale and full-scale SBR corporate-fed phased arrays are analyzed. Upper-bound DPCA clutter cancellation capability, in terms of radiation pattern match, is presented. The influence of main beam scan angle, array illumination, phase center displacement, array size, array lattice, number of passively terminated element guard bands, and radiating element type on two-phase center DPCA clutter cancellation is investigated. Dipole and monopole arrays having square and hexagonal lattices are analyzed. It is shown quantitatively that variation of the above array parameters can influence substantially the DPCA clutter cancellation.

ACKNOWLEDGEMENTS

We wish to express our gratitude to S.E. French for running the computer simulations and plotting the theoretical results.

TABLE OF CONTENTS

ABSTRACT	iii
ACKNOWLEDGEMENTS	v
LIST OF ILLUSTRATIONS	ix
1. INTRODUCTION	1
2. THEORY	11
2.1 Method of Moments	11
2.2 Displaced Phase Center Antenna Clutter Cancellation	16
3. RESULTS	19
3.1 Introduction	19
3.2 Sub-scale SBR 96-Element Planar Phased Array	19
3.3 Sub-scale SBR 32-Element Linear Phased Array	27
3.4 Sub-Scale and Full-Scale SBR Planar Phased Arrays	34
4. CONCLUSION	47
APPENDIX A - DERIVATION OF CLUTTER CANCELLATION FACTOR	49
REFERENCES	53

LIST OF ILLUSTRATIONS

Figure No.		Page
1-1	Two-Phase Center DPCA Radar Platform Showing Transmit and Receive Phase Centers for Consecutive Pulses	2
1-2	Amplitude Illumination For Two-Phase Center DPCA: (a) Overlapped Receive Apertures and (b) Split Receive Apertures	4
1-3	Corporate Feed for Two Phase Centers	5
1-4	Illustration of Asymmetry in Array Mutual Coupling Environment for Forward and Trailing Phase Centers	6
1-5	Array Antenna Elements and Center Element Radiation Patterns: (a) Monopoles and (b) Dipoles	8
2-1	Geometry for Finite Array Antennas. (a) Monopole Array Over Ground Plane, (b) Equivalent Dipole Array with Ground Plane Removed and Monopole Images Included, (c) Horizontal Dipole Array over Ground Plane, and (d) Equivalent Dipole Array with Ground Plane Removed and Dipole Images Included	12
2-2	Geometry for Arbitrarily Oriented Dipole Antenna in Free Space	14
2-3	Circuit Model for Array Antenna	15
2-4	Geometry for Nadir-Pointed Space-Based Radar Antenna	18
3-1	Ninety-Six-Element DPCA Test Array	20
3-2	Ninety-Six-Element DPCA Test Array Layout: (a) Experimental Array and (b) Theoretical Array	21
3-3	Transmit Radiation Pattern Using -10 dB Cosine Taper for the 96-Element Monopole Test Array. Scan Angle Is $\theta = 50^\circ$	23
3-4	Receive Array Radiation Patterns Using -10 dB Cosine Taper for the 96-Element Monopole Test Array. Phase Center Separation Is Three Columns. Scan Angle Is $\theta = 50^\circ$. (a) Amplitude and (b) Phase	24
3-5	Cancellation as a Function of Phase Center Displacement in Columns for the 96-Element Test Array. (a) Monopole Elements and (b) Dipole Elements	25

Figure No.		Page
3-6	Cancellation as a Function of Scan Angle Using Monopole and Dipole Elements with 3- and 6-Column Phase Center Separation for the 96-Element Test Array	26
3-7	Cancellation Versus Phase Center Displacement Difference (With No Guard Bands) for the 96-Element Test Array. (a) Monopole Elements and (b) Dipole Elements	28
3-8	Cancellation Versus Phase Center Displacement Difference (With Two Guard Bands) for the 96-Element Test Array. (a) Monopole Elements and (b) Dipole Elements	29
3-9	Cancellation Versus Number of Guard Bands for the 96-Element DPCA Array	30
3-10	Sub-Scale SBR 32-Element Linear Test Array with Monopole Elements. Thirty-Two Elements in the Center Row Are Used to Form the Transmit/Receive Patterns. Two Guard Bands of Passively Terminated Elements Surround the 32-Element Linear Array	31
3-11	Transmit Radiation Pattern Using Uniform Illumination for the 32-Element Monopole Test Array. Scan Angle Is $\theta = 50^\circ$	32
3-12	Receive Array Radiation Patterns Using -40 dB Taylor Taper for the 32-Element Monopole Test Array. Phase Center Separation Is Eight Columns. Scan Angle Is $\theta = 50^\circ$. (a) Amplitude and (b) Phase	33
3-13	Cancellation as a Function of Phase Center Displacement in Columns for the 32-Element Test Array. (a) Monopole Elements and (b) Dipole Elements	35
3-14	Cancellation as a Function of Scan Angle Using Different Array Illuminations with 8- and 16-Column Phase Center Separation for the 32-Element Test Array. (a) Monopole Elements and (b) Dipole Elements	36
3-15	Cancellation as a Function of Scan Angle Using Monopole and Dipole Array Elements with 8- and 16-Column Phase Center Separation for the 32-Element Test Array. (a) Uniform Transmit Illumination/40 dB Taylor Receive Illumination. (b) Cosine Transmit/Receive Illumination with 10 dB Edge Taper	37
3-16	Cancellation Versus Number of Guard Bands for the 32-Element DPCA Array	38

Figure No.		Page
3-17	Sub-Scale and Full-Scale Array Geometry. The Number of Active Rows Is Fixed at Eight. The Number of Active Columns Is Variable. Two Guard Bands Surround the Active Array	39
3-18	Cancellation as a Function of Number of Active Array Columns for One-Half Aperture Phase Center Spacing Using Monopole and Dipole Antenna Elements. (a) Square Lattice and (b) Hexagonal Lattice	41
3-19	Cancellation as a Function of Number of Active Array Columns for One-Half Aperture Phase Center Spacing Using Square and Hexagonal Array Lattices. (a) Monopole Elements and (b) Dipole Elements	42
3-20	Cancellation as a Function of Array Length for One-Half Aperture Phase Center Spacing Using Square and Hexagonal Array Lattices. (a) Monopole Elements and (b) Dipole Elements	43
3-21	Cancellation Versus Phase Center Displacement in Columns for an 8 Active Row By 128 Active Column DPCA Array	44
3-22	Cancellation Versus Number of Active Rows in an Array Having 128 Active Columns	45
3-23	Cancellation Versus Number of Guard Bands for an 8 Active Row by 128 Active Column DPCA Array	46

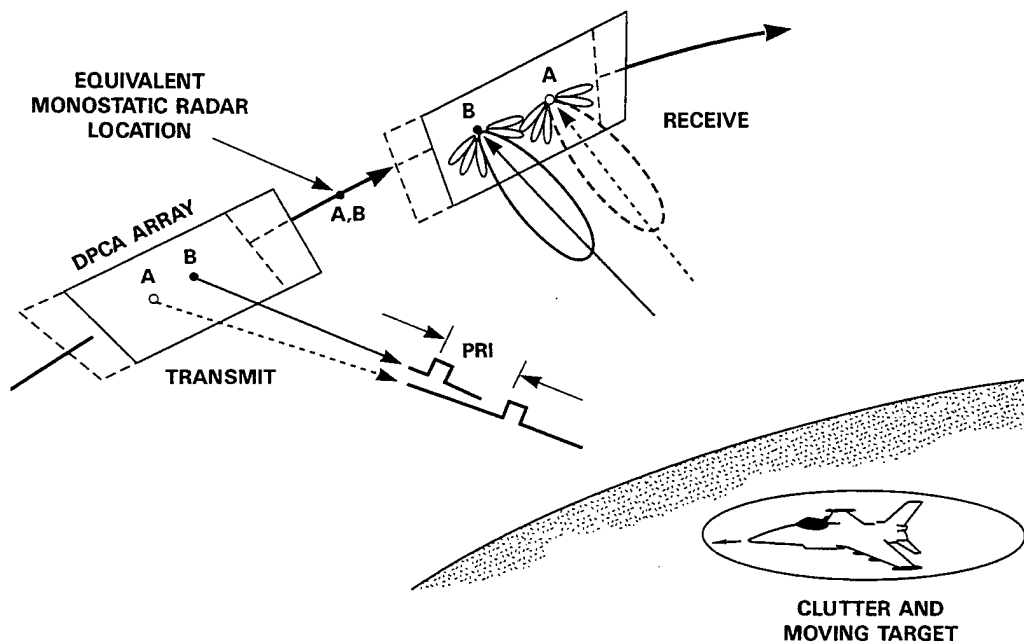
1. INTRODUCTION

In airborne or spaceborne radar systems applications, moving target indicator (MTI) techniques are used to distinguish scatterers containing a velocity component above some minimum detectable velocity (MDV) from those scatterers moving at speeds less than the MDV. Two well-known MTI techniques are pulse Doppler (PD) and displaced phase center antenna (DPCA). In a pulse Doppler radar system, the antenna main beam width is used to separate desired targets (above the MDV) from clutter or scatterers moving at less than the MDV. With DPCA, ground clutter is cancelled by utilizing appropriate signal generation/processing and two (or more) independent precision-matched radiation patterns generated by a single antenna [1,2].

The displaced phase center antenna concept has application in the design of a space-based radar (SBR) system [3]. Clutter cancellation of 40 to 50 dB is often discussed in the SBR context. A two-phase center DPCA system is depicted in Figure 1-1, where a moving target and a moving SBR DPCA platform are shown. Here, the full aperture is used for two successive pulse transmissions and, on receive, two displaced portions of the aperture are used. The phase center displacement between the receive apertures is adjusted to compensate for the platform velocity. Thus, for two pulses separated in time by one pulse repetition interval (PRI) the first reception occurs at the forward phase center. During a PRI, the clutter is effectively stationary; however, during this interval the target moves. Due to this movement, the target has a relative phase shift. There is no such phase shift from the clutter during this time. In simplistic terms, when the signals received by the two phase centers are subtracted, the clutter is significantly cancelled. The corresponding target return depends on the amount of target phase shift in one PRI. The amount of clutter cancellation achieved is limited by how well the two phase center radiation patterns are matched, in amplitude and phase, primarily over the main beam. The main beam pattern match is affected by array geometry and scan conditions (due to array element mutual coupling), and hardware tolerances (such as the transmit/receive (T/R) modules and the beamformer). In this report, the effects of array mutual coupling alone are considered. Other common sources of error (phase-center offset, antenna deformation, receiver channel mismatch, T/R module amplitude and phase errors, etc.) have been analyzed by Miller [4].

The displacement (separation) between the phase centers of the two receive antennas is denoted by Δ . To achieve the desired clutter cancellation, this separation must be related to the PRI of the radar waveform by the "DPCA condition"

$$\Delta = 2V_p T, \quad (1.1)$$



128883-20

Figure 1-1. Two-phase center DPCA radar platform showing transmit and receive phase centers for consecutive pulses.

where T is the PRI and V_p is the platform speed [5]. To eliminate the blind speeds associated with a simple pulse-train waveform, a practical system will base target detection on a non-coherent combination of many coherent processing intervals, each with a slightly different PRI, chosen according to a suitable algorithm. Thus, a range of phase center separations, typically varying by a factor of two between largest and smallest, must be provided by the antenna system.

Movement of the phase centers in a displaced phase center antenna is accomplished using amplitude illumination control. Consider Figure 1-2 which depicts two examples for displaced receive apertures - overlapped and split. The phase center displacement is denoted by the symbol Δ . As Δ increases, the size of each phase center subaperture decreases. Hence, the width of the receive antenna main beam increases as the phase center displacement increases. Phase center displacement in a phased array antenna is conveniently effected by means of attenuators in the transmit/receive modules. Unused elements in the phase center are "turned off" to a large value of attenuation, typically in a matched load impedance. After performing amplitude and phase weighting in each module, the received signals in each phase center are summed in a coherent power combiner (corporate feed) as shown in Figure 1-3. Notice that array mutual coupling is represented by the curved arrows emerging from the various array elements.

It has already been mentioned that module errors will not be treated in this report. If there was no array mutual coupling as well, then the radiation patterns generated by two subapertures would be identical. However, array mutual coupling is always present in a practical antenna and this leads to mismatch in the displaced phase center antenna aperture illumination functions and, thus, the patterns as well. The reason for this can be easily seen in referring to Figure 1-4 where the two subarrays are fully split apart. There is a mirror symmetry in the subarray geometries with respect to the boundary line between the forward and trailing phase centers. For example, the forward phase center has as many terminated elements to its left as the trailing subarray has to its right. However, the subarrays are not symmetrically surrounded by terminated elements. In an infinite array, even with mutual coupling, forward and trailing subarrays would produce radiation patterns which are perfectly matched. Since, in practice, the subarrays are embedded within a finite array, array edge effects will cause the forward and trailing subarray radiation patterns to become mismatched. Guard bands of passively terminated elements will tend to restore the symmetry of the two phase centers. Note that guard bands are commonly used to provide impedance matching to edge elements of a phased array antenna.

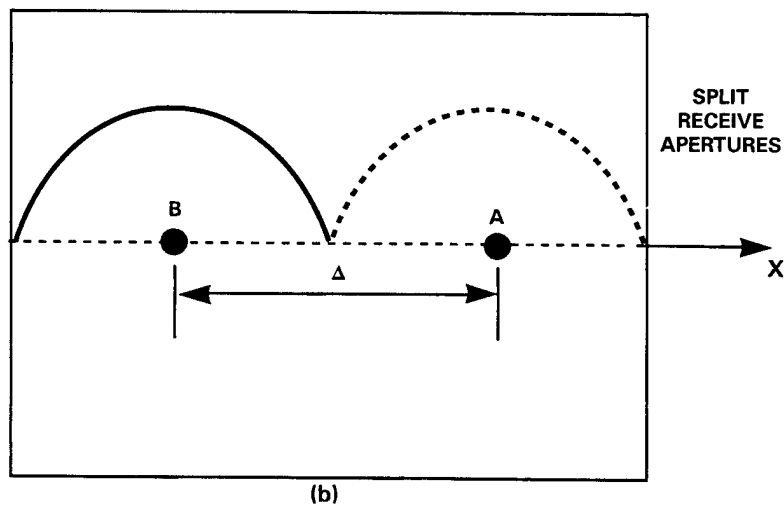
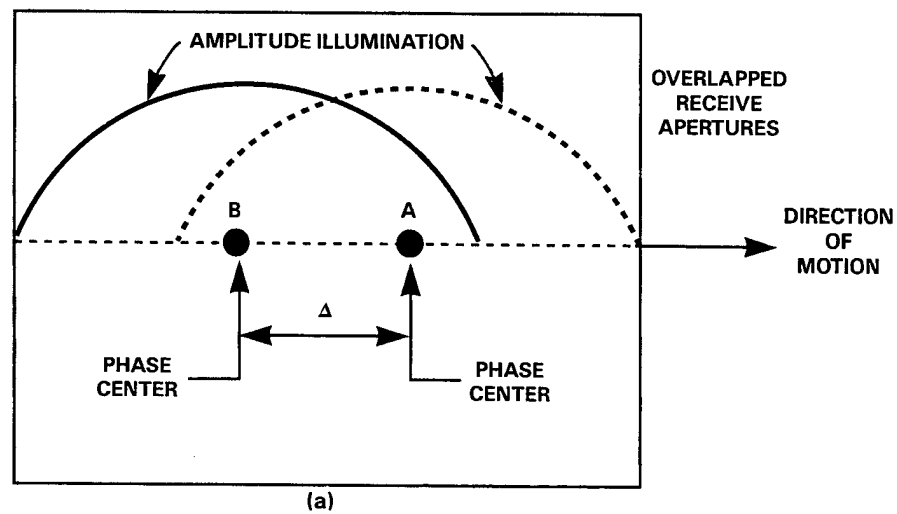


Figure 1-2. Amplitude illumination for two-phase center DPCA: (a) overlapped receive apertures and (b) split receive apertures.

128883-19

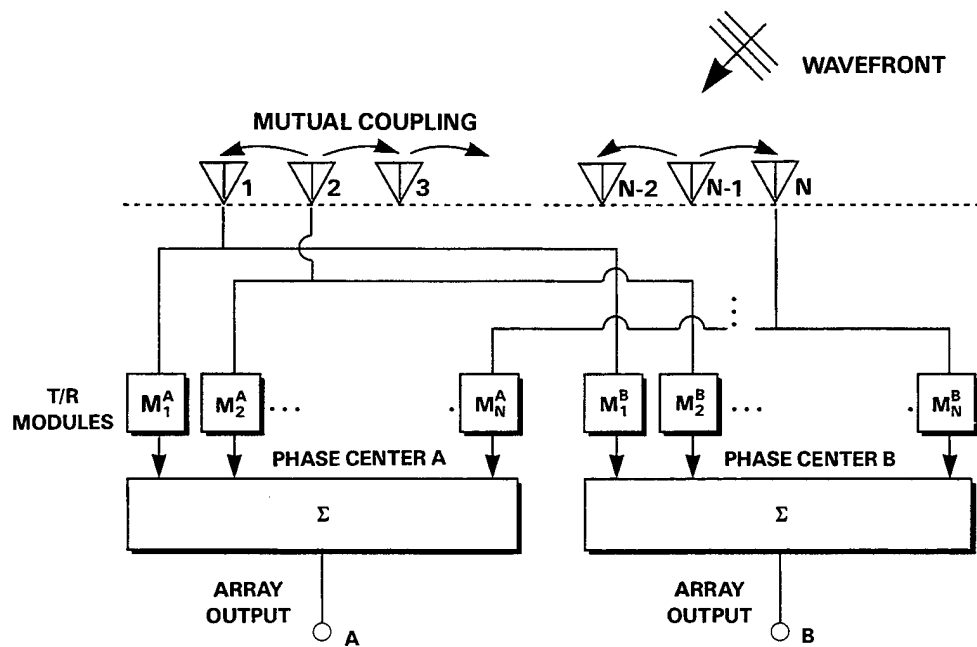
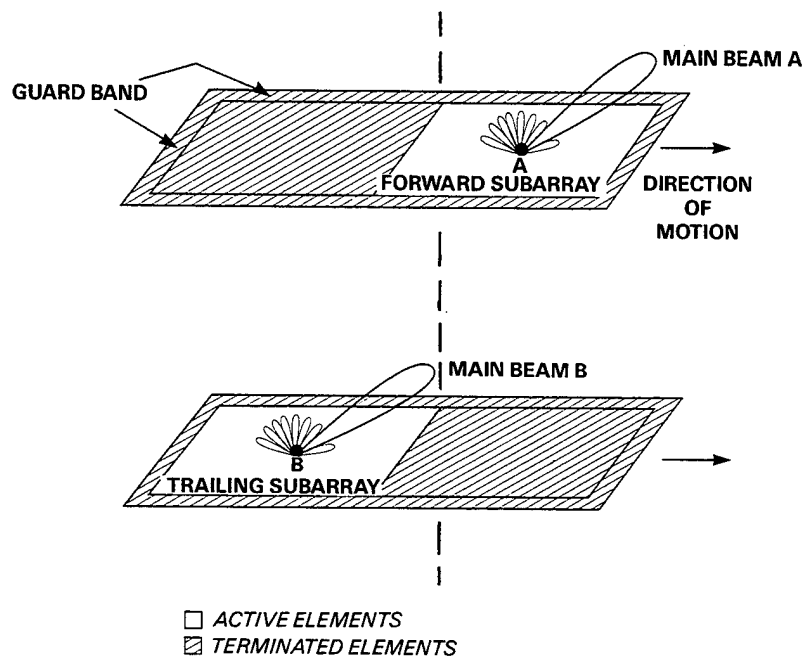


Figure 1-3. Corporate feed for two phase centers.



128883-18

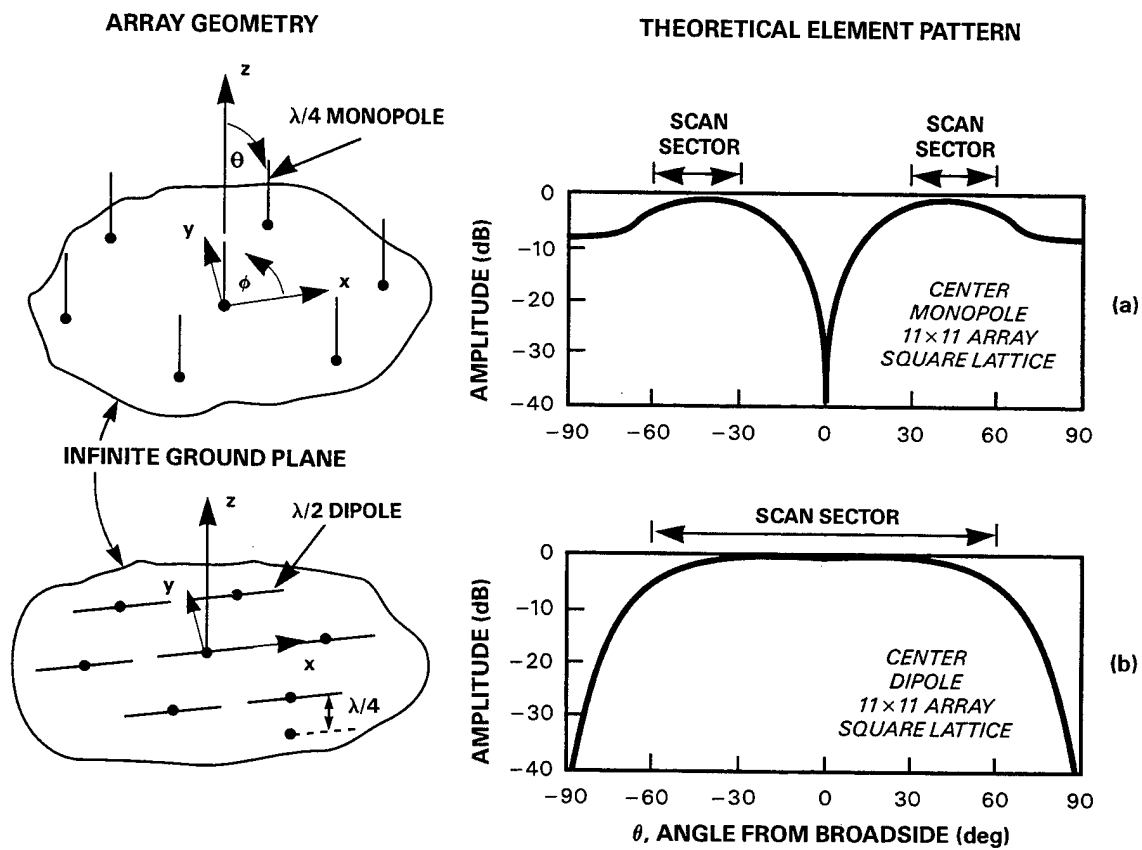
Figure 1-4. Illustration of asymmetry in array mutual coupling environment for forward and trailing phase centers.

An experimental sub-scale SBR DPCA phased array has recently been built. The active portion of the antenna consists of 96 monopole elements arranged in a hexagonal lattice having 8 rows and 12 columns. Two guard bands of passively terminated elements surround the 96-element active array to reduce edge effects. Using various measurement techniques [6,7], limited DPCA testing of this antenna has been performed. Many questions remain regarding the possible influence of phased array antenna design on DPCA clutter cancellation. Fundamental design parameters for a DPCA phased array are:

- size of array
- type of array antenna elements
- array lattice
- number of passively terminated element rows (guard bands)
- phase center displacement
- scan sector

To quantify the effects of varying these design parameters experimentally would require a great deal of effort. In contrast, theoretical calculations involving changes in the array design parameters can easily be accomplished. It was decided then, in order to gain a better understanding of how phased array antenna design affects DPCA clutter cancellation performance, to perform a detailed theoretical study. Both sub-scale and full-scale SBR antenna designs are examined in this report. Only corporate-fed phased arrays will be examined here. Space-fed lens DPCA phased arrays are examined briefly in reference 12. Antenna array elements typically considered for the SBR application are monopoles (broadside null) and dipoles (broadside maximum) [8]. These antenna elements are readily analyzed using the method of moments [9-11]. Figure 1-5 shows monopole and dipole antenna elements and their theoretical center element patterns in an array. In computing these radiation patterns, an 11-row by 11-column array with a square lattice has been assumed. Notice that the monopole has a null at broadside compared to the dipole which has a peak at broadside. The useable scan sector for an array of monopoles is from 30 to 60° from broadside. In contrast, the dipole array scan sector covers 0 to 60° from broadside. Monopoles are sometimes considered for a low-altitude space-based radar system where the broadside null is actually useful in reducing the nadir (high grazing angle) clutter. The method of moments is known to be accurate in predicting the performance of monopole and dipole arrays. For example, the input impedance and radiation patterns of monopole phased arrays have been computed, recently, using the method of moments and are in good agreement with measurements [9].

This report is organized as follows: In Section 2, a brief description of the theory is given. In Section 3, results are presented for sub-scale and full-scale SBR DPCA arrays.



128883-24

Figure 1-5. Array antenna elements and center element radiation patterns: (a) monopoles and (b) dipoles.

The effects of scan angle, phase center displacement, type of radiating element, and number of passively terminated guard bands are examined in detail. A sub-scale SBR 96-element planar array is described and analyzed in Section 3.1. Comparisons of theory and available measured data are made. In Section 3.2, a sub-scale SBR 32-element linear array is studied. Sub-scale and full-scale SBR arrays, up to a size of 16 meters, are investigated in Section 3.3. The results presented in this report make it possible to place an *upper bound* (due to array mutual coupling effects) on the DPCA cancellation which can be achieved with a given size array antenna. The situation of more than two phase centers is readily handled under the theoretical framework presented here; however, only two-phase center DPCA is investigated in this report.

2. THEORY

2.1 METHOD OF MOMENTS

As mentioned earlier, in this report both dipole and monopole arrays over an infinite ground plane will be analyzed. Bandwidth effects will not be addressed in this report and so optimization of the element design is not under consideration. The two basic array elements, $\lambda/2$ dipole and $\lambda/4$ monopole (where λ is the wavelength), are depicted in Figure 2-1. These elements are assumed to be thin cylindrical wire antennas close to resonance, which allows a convenient formulation of the method of moments. A previous report [10] has given a moment method formulation for monopole arrays. A very similar formulation can be given for dipole arrays. The mathematical details of the formulation will be covered only briefly here.

In the method of moments, boundary conditions are used to find the antenna response (current) to a given excitation (voltage). The excitation here is the amplitude and phase incident at each element of the phased array. Due to mutual coupling or the mutual impedance between array elements, the actual illumination achieved will be different from the theoretical desired. It is this deviation from the ideal that DPCA performance will depend on.

It is assumed that there is one unknown complex current per element of the array. The current distribution is assumed to be piecewise sinusoidal. This current distribution is used as the moment method basis and testing functions. When the basis functions and testing functions are the same, this is known as a Galerkin's formulation. For a piecewise-sinusoidal Galerkin's moment method formulation, the mutual impedance between array elements is readily computed [13].

The geometry for a finite array of dipoles or monopoles over ground plane is shown in Figure 2-1. Standard spherical coordinate angles (θ, ϕ) are used to describe the observation position for far-field pattern computation. The ground plane is located in the $z = 0$ plane. The dipoles are \hat{x} polarized and the monopoles are \hat{z} polarized. Using image theory, the ground plane can be removed from the analysis. For a monopole array, an equivalent dipole array results (Figure 2-1(b)). For a dipole array, removal of the ground plane is accomplished by adding an image array of dipoles (Figure 2-1(d)). In theory, the monopole radiates (or receives) only the E_θ electric field component. In the $\phi = 0^\circ$ plane, the principal polarization for the dipole is the E_θ component. In the $\phi = 90^\circ$ plane, the dipole principal polarization is the E_ϕ component. However, for a radar application, the slant-linear polarization (total electric field) is of interest. The radiation pattern of a vertical dipole is well known and is expressed (in primed coordinates) as

$$E_{\theta'} = j60i_n P_{\theta'}(\theta') \quad (2.1)$$

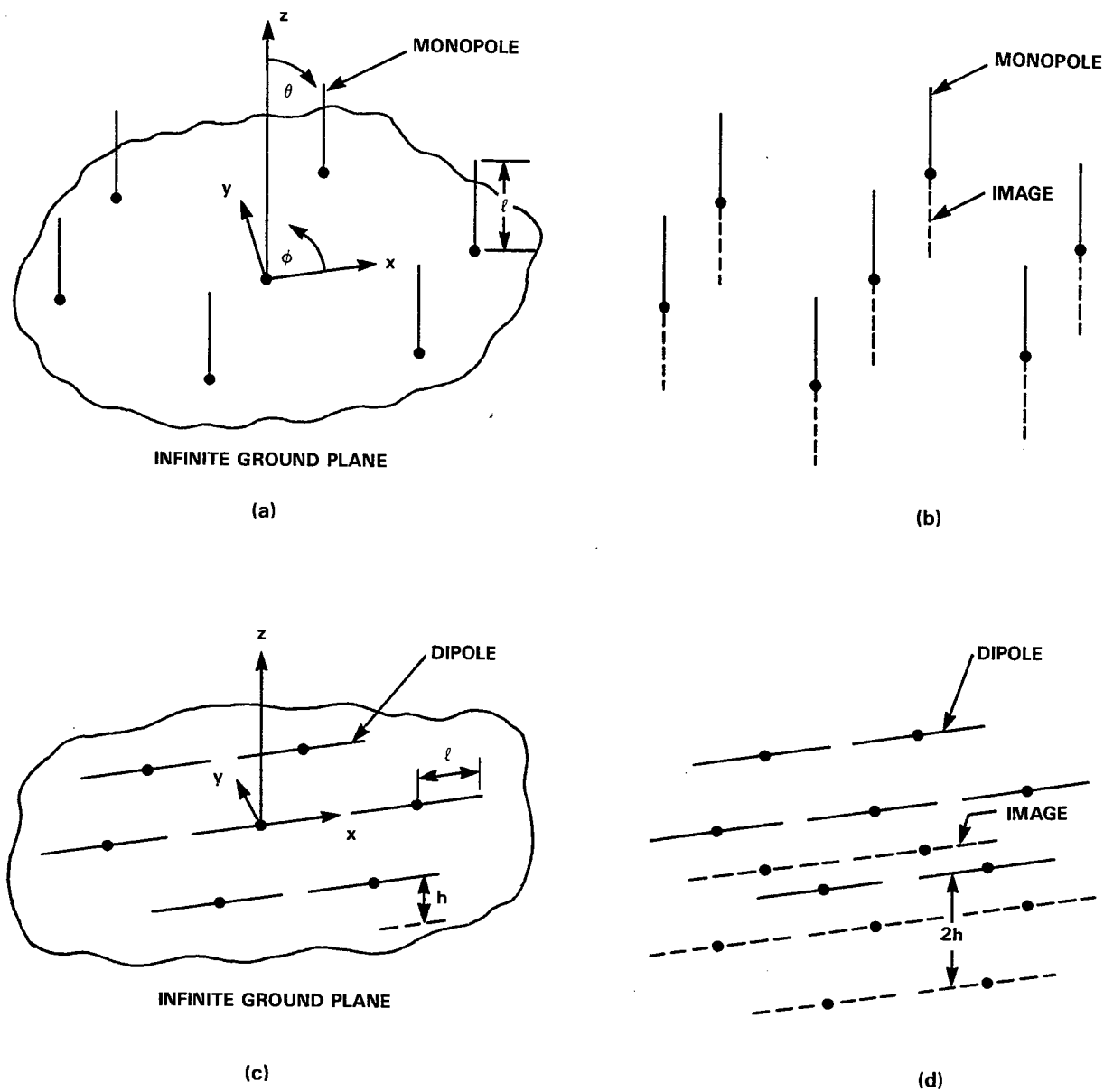


Figure 2-1. Geometry for finite array antennas. (a) monopole array over ground plane, (b) equivalent dipole array with ground plane removed and monopole images included, (c) horizontal dipole array over ground plane, and (d) equivalent dipole array with ground plane removed and dipole images included.

where i_n is the complex terminal current for the n th element and $P_{\theta'}$ is the isolated-element normalized pattern which is given by

$$P_{\theta'} = \frac{\cos(\beta l \cos \theta') - \cos(\beta l)}{\sin(\beta l) \sin \theta'} \quad (2.2)$$

where l is the dipole half-length, and $\beta = 2\pi/\lambda$ is the propagation constant. It has been assumed that the vertical dipole is \hat{z}' oriented with θ' being the angle measured from the axis of the dipole, as shown in Figure 2-2. Equation (2.1) is the required expression used to compute the isolated element pattern for either a monopole array or dipole array. This expression is the desired slant-linear polarization component of the electric field. To compute the array pattern including mutual coupling effects it is necessary to compute the array terminal currents defined above.

Consider Figure 2-3 which shows a circuit model for two elements (m, n) of an array operating in the transmit mode. The driving source is a voltage generator in series with a generator impedance. The generator and impedance load are connected to the terminals of a radiating antenna element which has a self-impedance and a mutual impedance with respect to every element of the array. Let \mathbf{Z} represent the mutual impedance matrix for the array. Referring to Figure 2-3, \mathbf{Z} is expressed as

$$\mathbf{Z} = \mathbf{Z}^{o.c.} + \mathbf{Z}_L \mathbf{I} \quad (2.3)$$

where $\mathbf{Z}^{o.c.}$ is the open-circuit mutual impedance matrix for the array, \mathbf{I} is the identity matrix, and \mathbf{Z}_L is the load impedance. Define \mathbf{v} as the voltage excitation matrix of the array. Then the array element terminal currents, denoted \mathbf{i} , are found by solving the system of equations written in matrix form as

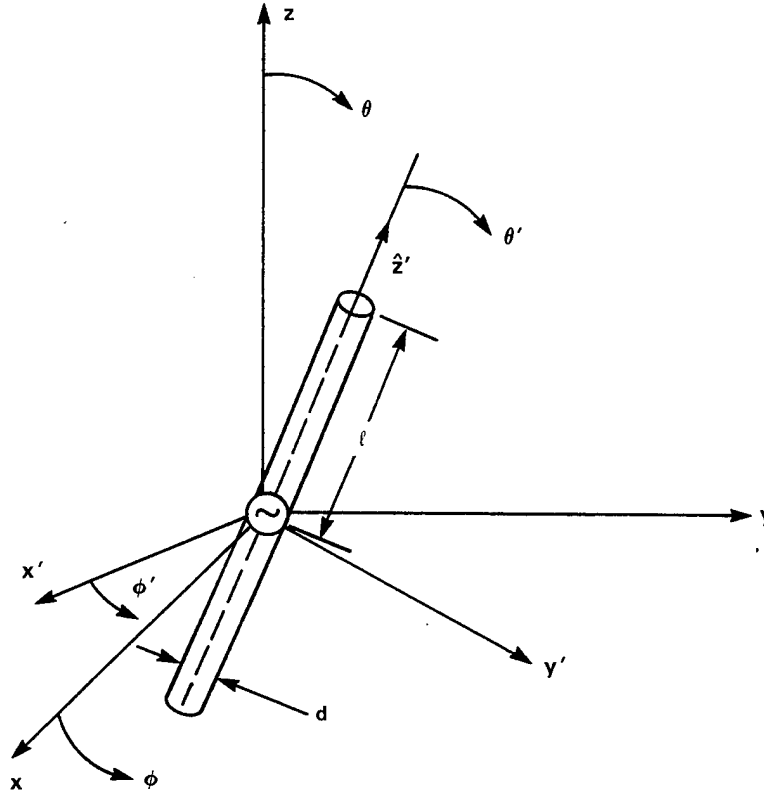
$$\mathbf{v} = \mathbf{Z} \cdot \mathbf{i}. \quad (2.4)$$

Upon calculating the array terminal currents, the array radiation pattern including mutual coupling is expressed as

$$E_{\theta'}^{array} = j60 P_{\theta'} \cdot AF \quad (2.5)$$

where $P_{\theta'}$ is given by Equation (2.1) and AF is the array factor which is given by

$$AF = \sum_{n=1}^N i_n e^{j\beta(\sin \theta(x_n \cos \phi + y_n \sin \phi) + z_n \cos \theta)} \quad (2.6)$$



128883-13

Figure 2-2. Geometry for arbitrarily oriented dipole antenna in free space.

where (x_n, y_n, z_n) are the coordinates for the terminals of the n th element and i_n is the moment method terminal current for the n th element.

Finally, the relation between the observation angles (θ, ϕ) and θ' is determined as follows: The dot product of the unit vectors in the dipole direction and the radial direction is simply,

$$\hat{z}' \cdot \hat{r} = \cos\theta'. \quad (2.7)$$

Next, the unit vector in the radial direction is expressed in terms of the rectangular coordinate system unit vectors as

$$\hat{r} = \sin\theta\cos\phi\hat{x} + \sin\theta\sin\phi\hat{y} + \cos\theta\hat{z}. \quad (2.8)$$

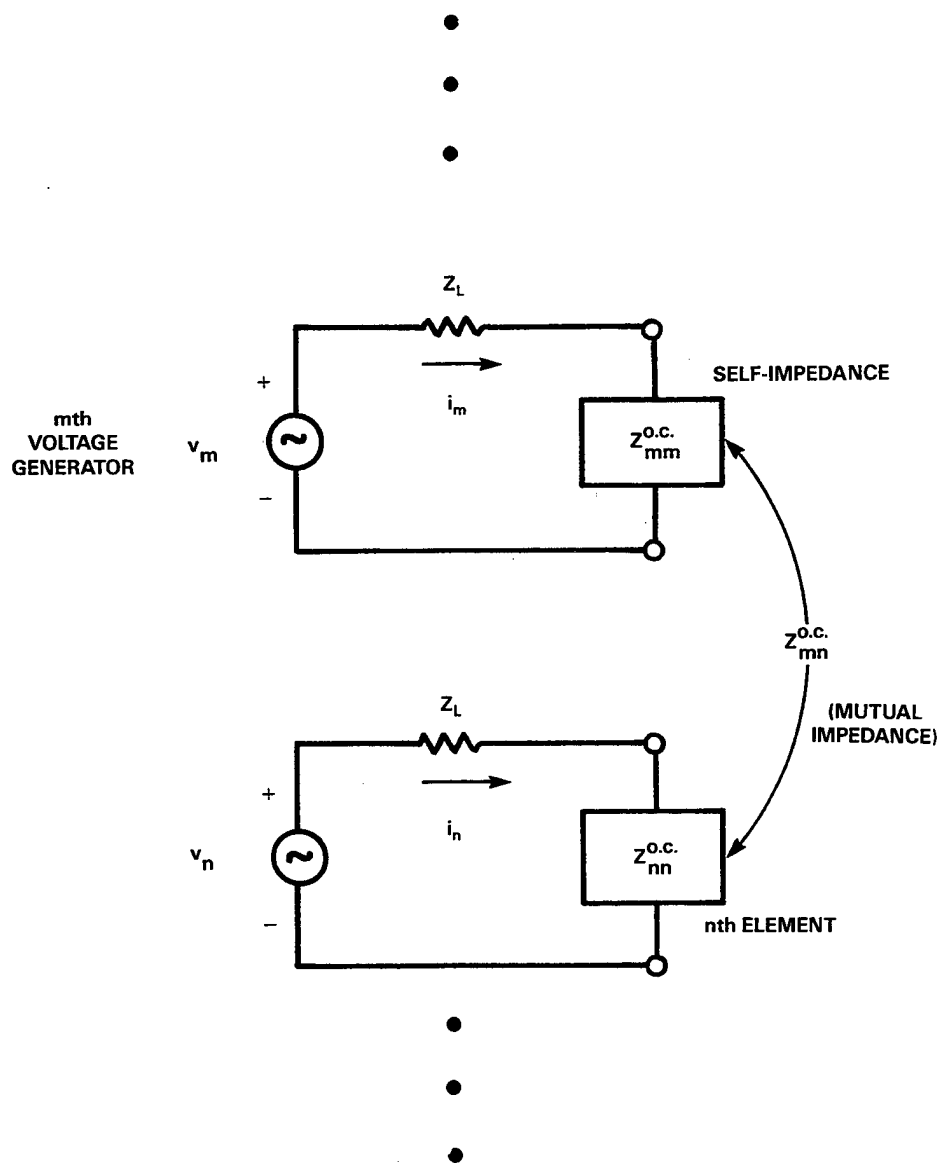


Figure 2-3. Circuit model for array antenna.

For z-directed dipoles (monopole plus image) $\hat{z}' = \hat{z}$ so that Equations (2.7) and (2.8) produce

$$\theta'_{monopole} = \theta. \quad (2.9)$$

Similarly, for x-directed dipoles it follows that

$$\theta'_{dipole} = \cos^{-1}(\sin\theta\cos\phi). \quad (2.10)$$

2.2 DISPLACED PHASE CENTER ANTENNA CLUTTER CANCELLATION

To compute the clutter cancellation capability of two DPCA radiation patterns, it is necessary to form the pattern correlation matrix

$$\mathbf{M} = \begin{bmatrix} M_{11} & M_{12} \\ M_{21} & M_{22} \end{bmatrix} \quad (2.11)$$

where the correlation between two channels is expressed as

$$M_{ij} = \int \int |E_o(\theta, \phi)|^2 E_i(\theta, \phi) E_j^*(\theta, \phi) e^{j(\psi_x + \psi_y)} A(\theta, \phi) d\theta d\phi \quad (2.12)$$

where (θ, ϕ) are standard spherical coordinates, $i = 1, 2$, $j = 1, 2$, $E_o(\theta, \phi)$ is the electric field pattern of the transmitting antenna, $E_1(\theta, \phi)$ and $E_2(\theta, \phi)$ are the electric field patterns of the two receiving antennas (* denotes conjugate), $A(\theta, \phi)$ is a weighting function that depends on the radar waveform, the clutter model, and the geometry of the problem. In this report, it is assumed that $A(\theta, \phi) = 1$ so the clutter cancellation is dependent on the antenna pattern match only. The electric field patterns $E_1(\theta, \phi)$ and $E_2(\theta, \phi)$ are measured or computed with respect to their assumed phase center positions, which we take to be the geometric centers of the excited portions of the respective apertures. The phase functions ψ_x and ψ_y represent the effect of differences, in the longitudinal and transverse directions, between the separation of these phase centers and the values required to meet the DPCA condition mentioned earlier. The phase functions are expressed in terms of these spatial differences by the following equations

$$\psi_x = \frac{2\pi}{\lambda} \Delta_x \sin\theta \cos\phi \quad (2.13)$$

$$\psi_y = \frac{2\pi}{\lambda} \Delta_y \sin\theta \sin\phi \quad (2.14)$$

where Δ_x and Δ_y are the departures of the phase center separations, in the x (longitudinal) and y (transverse) directions, from the values required by the DPCA condition.

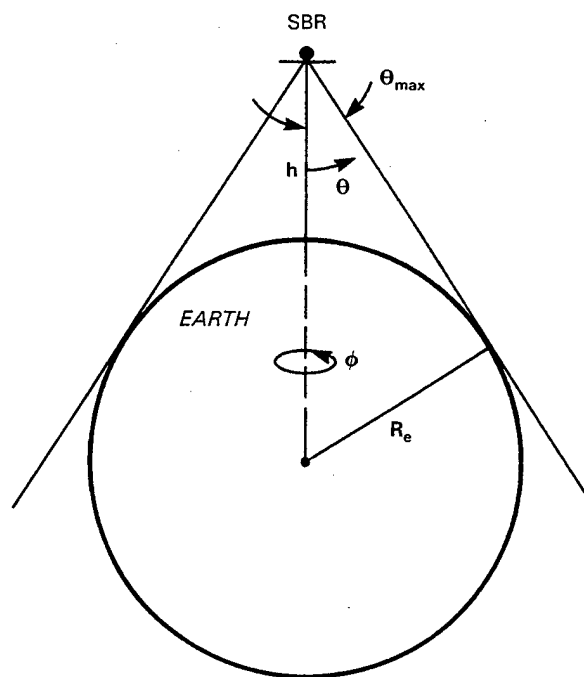
The latter condition demands no phase center separation in the transverse direction, assuming the phase centers are aligned with the direction of platform motion. Since the antenna excitations are normally symmetric in this direction, Δ_y is usually zero. The other component, Δ_x , can be nonzero for a variety of reasons. For example, the radar PRI may be incorrectly matched to the phase center separation. An example more relevant to this study occurs if the geometrical centers are not representative of the actual phase centers of the receive patterns. This will actually be the case when no guard bands are used, since mutual coupling will modify the effective excitations, causing the actual currents to be complex and shifting the phase centers. Illustrations of this effect are presented below. In any case, we are not concerned with academic definitions of phase center position, but with the proper choice of PRI to maximize clutter cancellation performance. With excitations distorted by mutual coupling, it is not easy to predict the best PRI for a given set of antenna excitations, and our examples will show that a departure from the geometrical spacing can sometimes improve performance significantly. In any case, if the best spacing is known (from theoretical analysis and/or testing), it is an easy matter to adjust the radar PRI to achieve it.

For a nadir-pointed SBR, as depicted in Figure 2-4, in Equation (2.12) the range of integration will be $0 < \phi < 2\pi$ and $0 < \theta < \theta_{max}$ where

$$\theta_{max} = \sin^{-1}\left(\frac{R_e}{R_e + h}\right) \quad (2.15)$$

where R_e is the radius of the Earth (this is taken to be 3440 nmi) and h is the altitude of the radar.

The DPCA arrangement with two phase centers may be viewed as an adaptive nulling system with two antenna channels. Since the two patterns are expected to be very well matched, and the pulse timing corresponds to the physical separation of their phase centers, the returns from stationary clutter should be nearly equal in the two channels. The target returns, however, will differ by a phase shift which is related to the actual target range rate (Doppler), and this phase determines the ideal steering vector in the two-channel system. It turns out, however, that nearly equal performance is attained when a single steering vector, $[1, 0]^T$ is used. This is a mismatched steering vector, but it suffices for all target range rates of interest, and hence simplifies the processing considerably. The performance of this two-channel nulling system depends, of course, on the true target Doppler (range rate) being very poor for targets with nearly zero Doppler, since these are lost in the clutter return. The optimum target range rate is one-half the radar blind speed, and detection performance is best for this case.



128833-11

Figure 2-4. Geometry for nadir-pointed space-based radar antenna.

The output SNR of this DPCA "nulling" system is, in any case, inversely proportional to the quantity

$$C = 1 - \frac{|M_{12}|^2}{M_{11}M_{22}} \quad (2.16)$$

which plays the role of a cancellation factor, reducing the clutter power perceived by the radar. The results presented in this report will all be expressed in terms of this quantity, since it can be related directly to system performance in the radar itself. A derivation of the above equation is given in Appendix A.

3. RESULTS

3.1 INTRODUCTION

In general, two-dimensional radiation patterns are required to completely evaluate the DPCA performance of an antenna (see Equation (2.12)). However, in this report only one-dimensional principal plane pattern cuts are used to calculate the DPCA performance, and Equation (2.12) is replaced by the corresponding one-dimensional integral. Simulations have shown that the one-dimensional pattern data yields cancellation results that are typically 3 to 4 dB higher than full two-dimensional data. Further, it is assumed here that the clutter is incident only from angles less than 60° from broadside. This is the geometry which would occur with a low-altitude SBR. To properly use the data which follows, it is desirable that the mutual-coupling limited (upper-bound) cancellation be at least 5 to 10 dB higher than the design goal. This is because of the assumption of one-dimensional data and the limited clutter cutoff angle.

3.2 SUB-SCALE SBR 96-ELEMENT PLANAR PHASED ARRAY

In this section, theoretical predictions of the upper-bound DPCA clutter cancellation for a sub-scale 96-element SBR phased array antenna are made. Previous reports [6,7] have discussed measured DPCA performance for an experimental L-band 96-element test array. Pertinent features of the antenna (array/element/module photographs and beamformer block diagram) are depicted in Figure 3-1. The experimental array consists of monopole antenna elements arranged in a hexagonal lattice with 5.0-inch spacing as depicted in Figure 3-2(a). The monopole length is $l = 2.3$ inches and the monopole diameter is $d = 0.125$ inch. The 96-element active receive portion of the array is surrounded by two guard bands of elements (the total number of guard elements is also 96). The array element spacing was chosen to allow a full conical scan to 60° from broadside. The operating frequency range for this array is 1.2 to 1.4 GHz with center frequency 1.3 GHz. The element spacing at center frequency is, thus, 0.55λ . The array amplitude and phase weighting was achieved using 6-bit phasers and 7-step (coarse) attenuators. Two independent beamformers (coherent power combiners) were used to implement two-phase center DPCA.

As mentioned earlier, with hardware it is often impractical to investigate the effects of varying the antenna array parameters, such as type of radiating element and number of guard bands. With software, variation of parameters is done relatively easy. In this section, comparisons of method of moments predictions and published measurements will be made where possible. Only a monopole array has been built and tested, but in the theoretical simulations monopoles and dipoles have been analyzed. A layout for the theoretical arrays

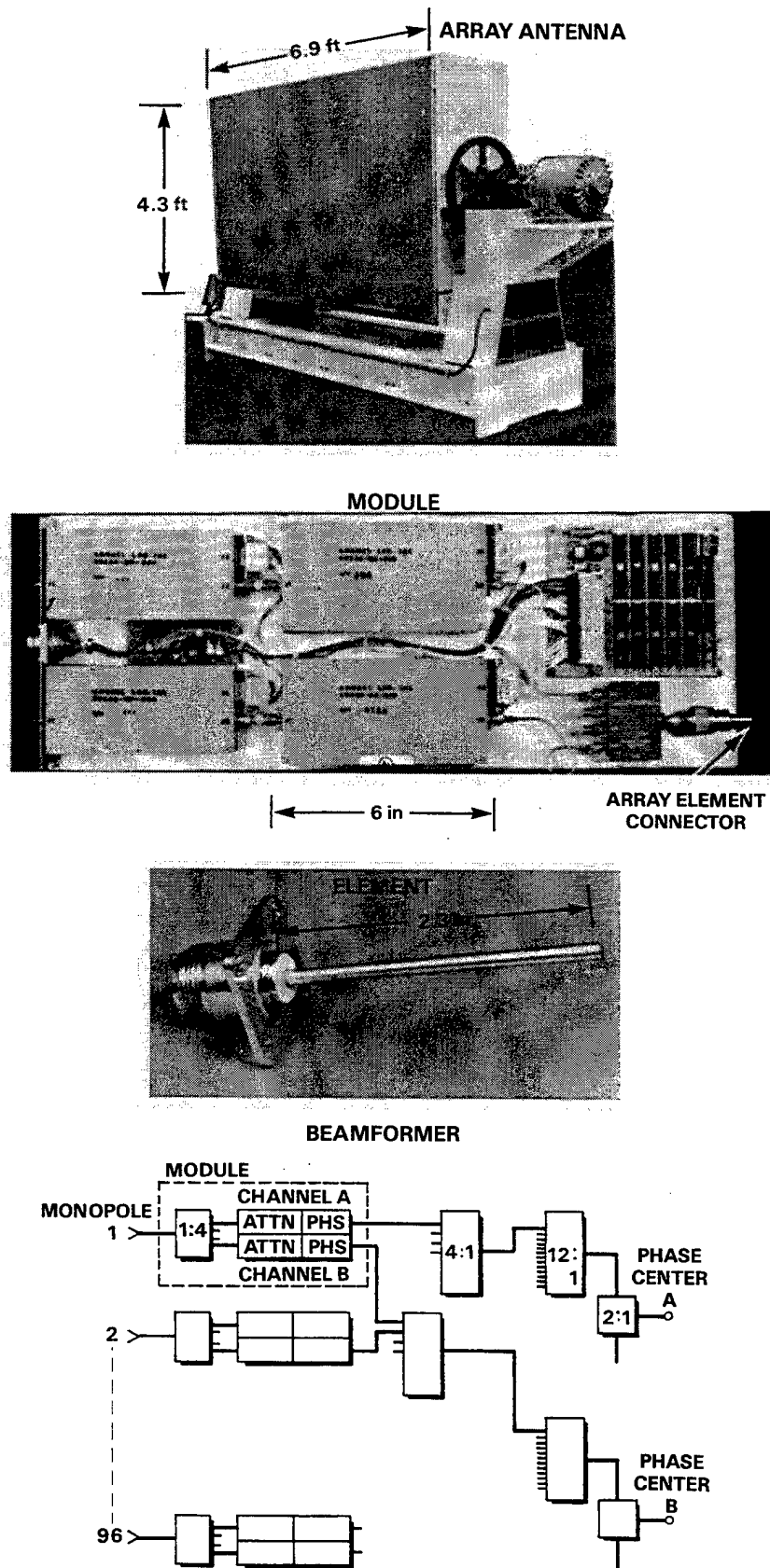


Figure 3-1. Ninety-six-element DPCA test array.

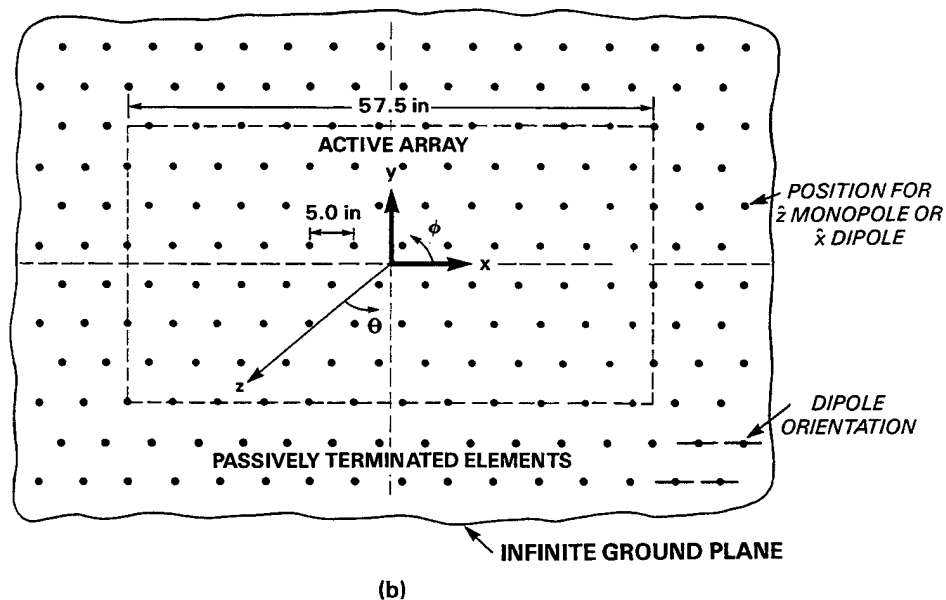
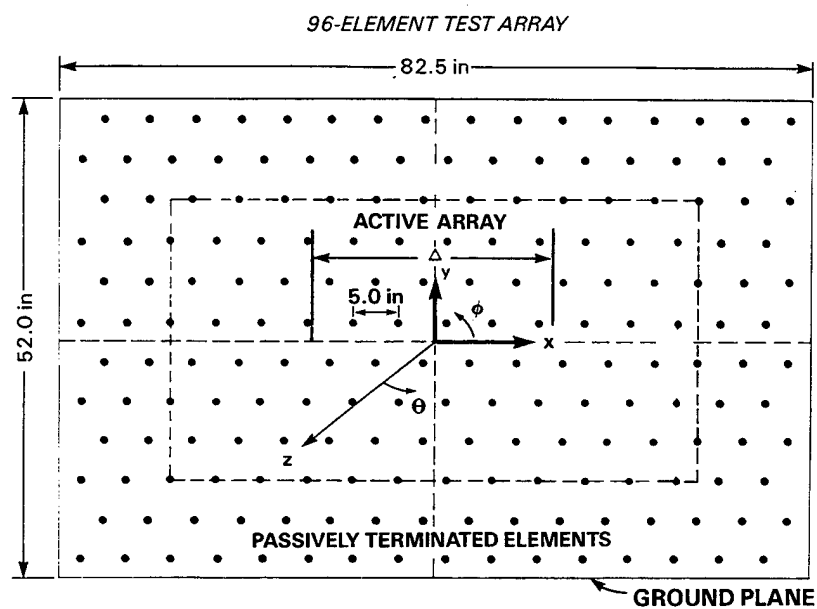


Figure 3-2. Ninety-six-element DPCA test array layout: (a) experimental array and (b) theoretical array.

is shown in Figure 3-2(b). Notice that the only difference between the experimental and theoretical monopole arrays is in the ground plane size - the experimental ground plane of course is finite and the theoretical ground plane has been assumed infinite. A finite ground plane could be included in the theory at the expense of more computation time. At present, the theory does not include any ground plane edge diffraction. The dipoles are assumed to have the same wire diameter as the monopoles. The dipole half-length is $l = 2.2$ inches and the spacing above ground plane is $h = 2.1$ inches.

Consider first the theoretical radiation patterns of the monopole array when steered to $\theta = 50^\circ$. Figure 3-3 shows the transmit pattern using a -10 dB cosine tapered (no pedestal) illumination. Figure 3-4(a,b) shows the receive patterns, amplitude and phase, respectively, for the case where the phase center separation is three columns (15.0 inches). (The receive illumination was also assumed to be a -10 dB cosine taper). The broadside null of the monopole is apparent in these patterns. Notice that the amplitude and phase of the two phase centers track very closely when $|\theta| < 60^\circ$. For $|\theta| > 60^\circ$ the two phase centers become mismatched. The importance of this is that the clutter cancellation capability is dependent on the selection of cutoff angle in the evaluation of Equation (2.12). Figure 3-4(a,b) clearly shows that the effect of mutual coupling is to create a mismatch between the two phase centers. Similar results are found for dipole elements.

Consider now, Figure 3-5(a,b) which shows the cancellation of monopole and dipole arrays for various scan angles ($\leq 55^\circ$) as a function of phase center displacement in columns. Notice that for both monopoles and dipoles the cancellation tends to slowly degrade as the phase center displacement increases. For this particular array design (8 by 12 elements, hexagonal lattice, two guard bands) it is observed that dipoles have a higher value of cancellation compared to monopoles.

For the monopole 40° scan case, experimental data for the test array was available. These data are also plotted in Figure 3-5(a) using the symbol (\bullet). Notice that the experimental data lies about 10 dB below the theoretical predictions. This is expected because the theory does not include any module errors; only mutual coupling effects. However, the variation as a function of phase center displacement is in good agreement. In other words, the theory is predicting the correct trend.

In Figure 3-6, the same theoretical results are replotted as a function of scan angle for both monopoles and dipoles with 3- and 6-column phase center displacements. For the monopole array, it can be concluded that the upper-bound cancellation is 50 dB at 40° scan, but only 30 dB at 55° scan. For a dipole array, the upper-bound cancellation is 48 dB at 40° scan and 40 dB at 55° scan.

One of the potential effects of mutual coupling is to shift the phase centers from their assumed positions, as mentioned in Section 2.2. The quantity Δ_x defined there, can be thought

128883-22

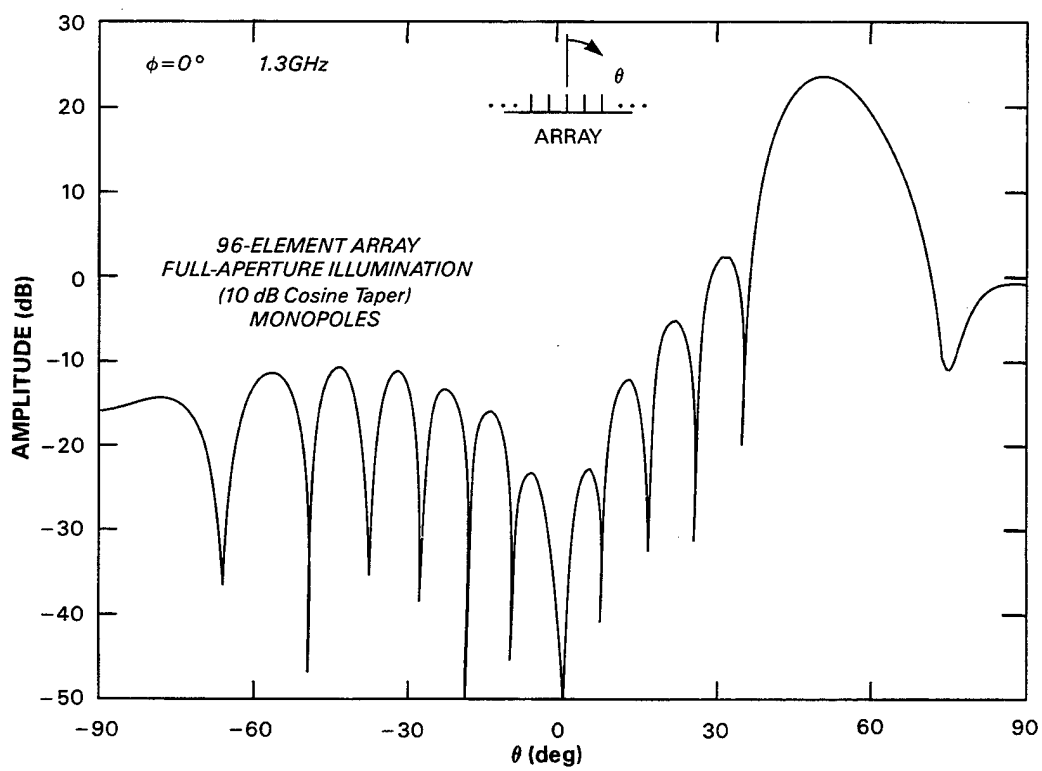
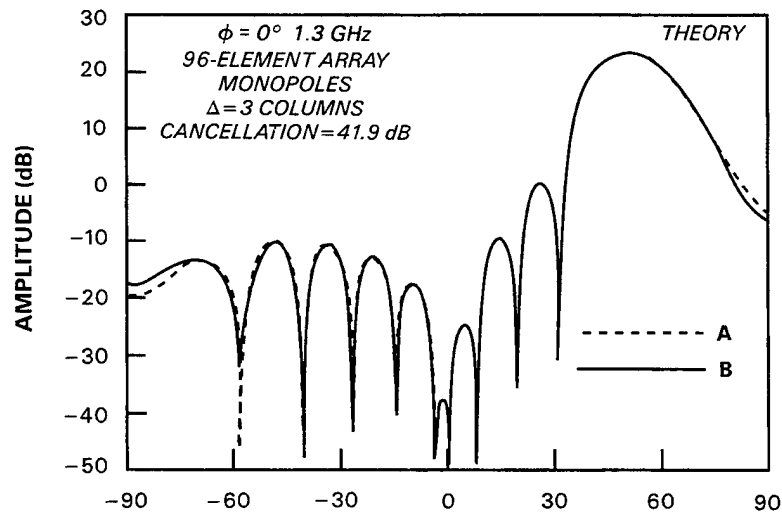
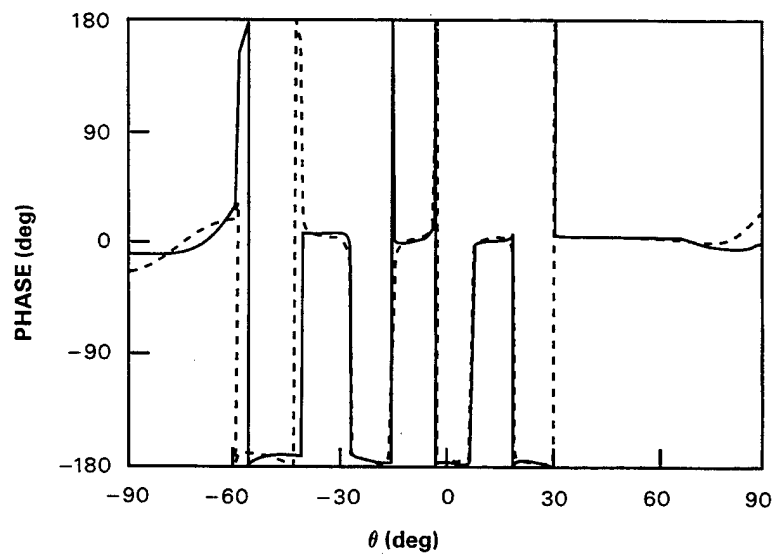


Figure 3-3. Transmit radiation pattern using -10 dB cosine taper for the 96-element monopole test array. Scan angle is $\theta = 50^\circ$.



(a)



(b)

Figure 3-4. Receive array radiation patterns using -10 dB cosine taper for the 96-element monopole test array. Phase center separation is three columns. Scan angle is $\theta = 50^\circ$. (a) amplitude and (b) phase.

128883-23

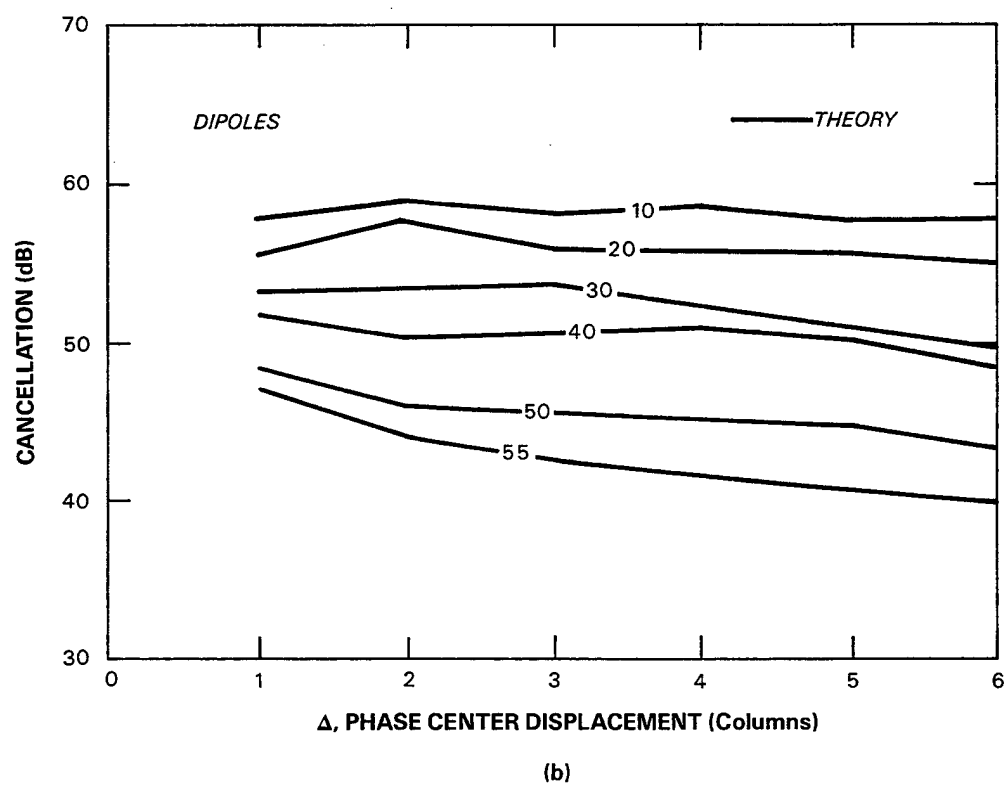
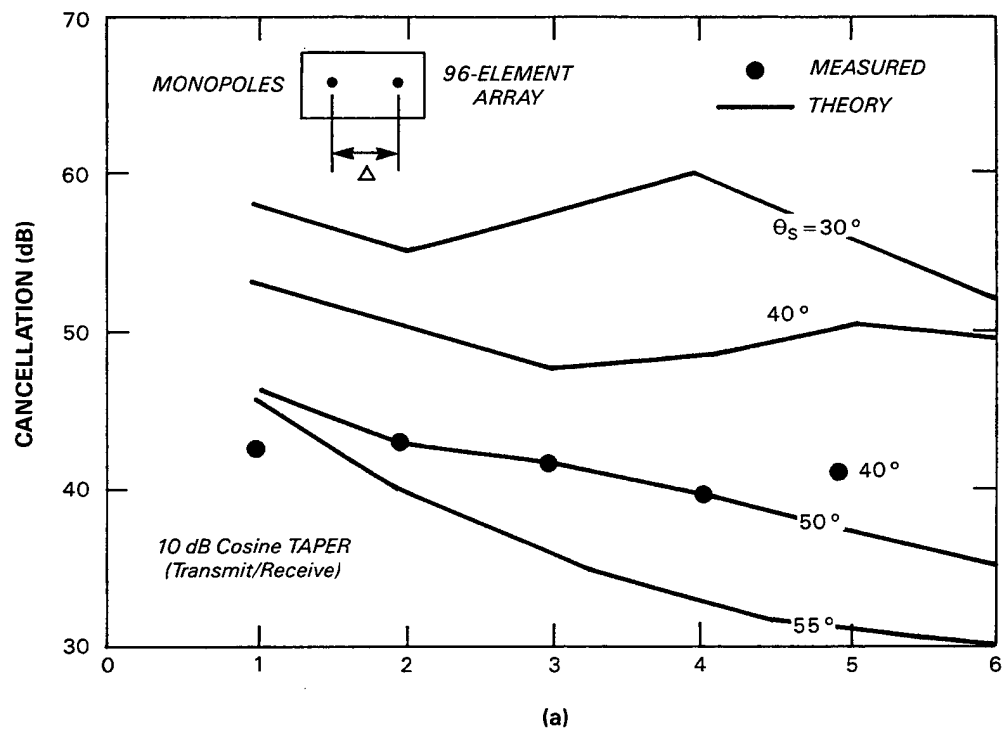
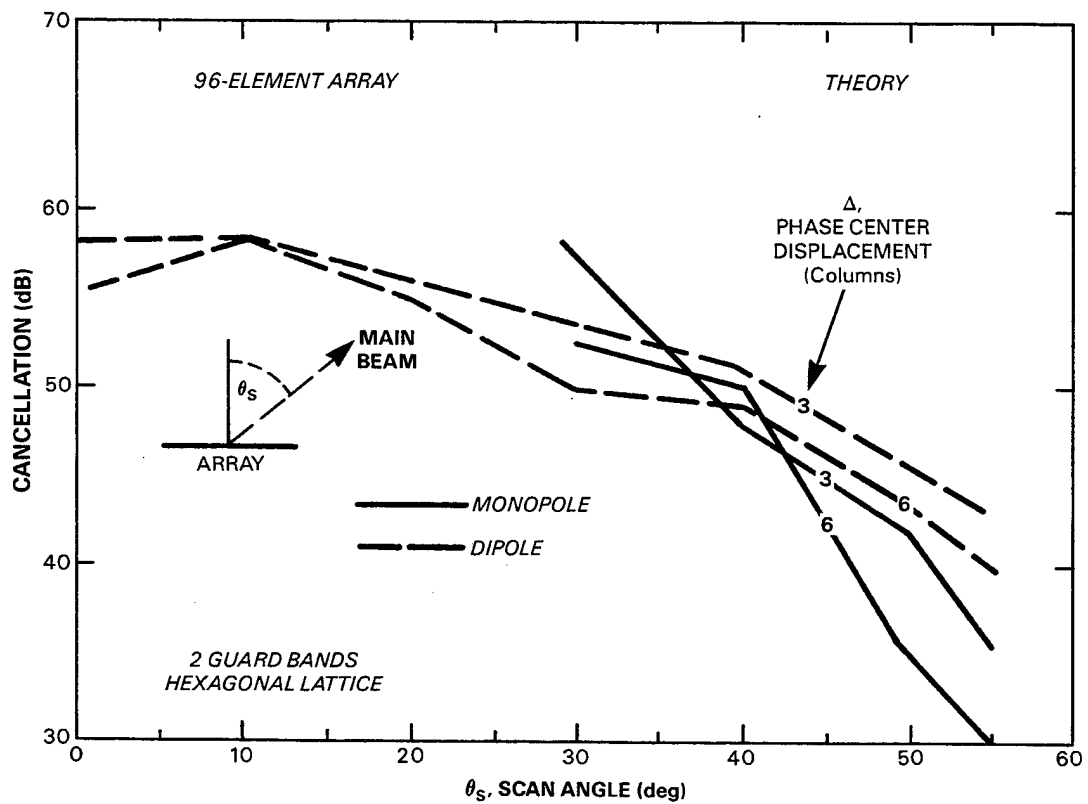


Figure 3-5. Cancellation as a function of phase center displacement in columns for the 96-element test array. (a) monopole elements and (b) dipole elements.



128883-28

Figure 3-6. Cancellation as a function of scan angle using monopole and dipole elements with 3- and 6-column phase center separation for the 96-element test array.

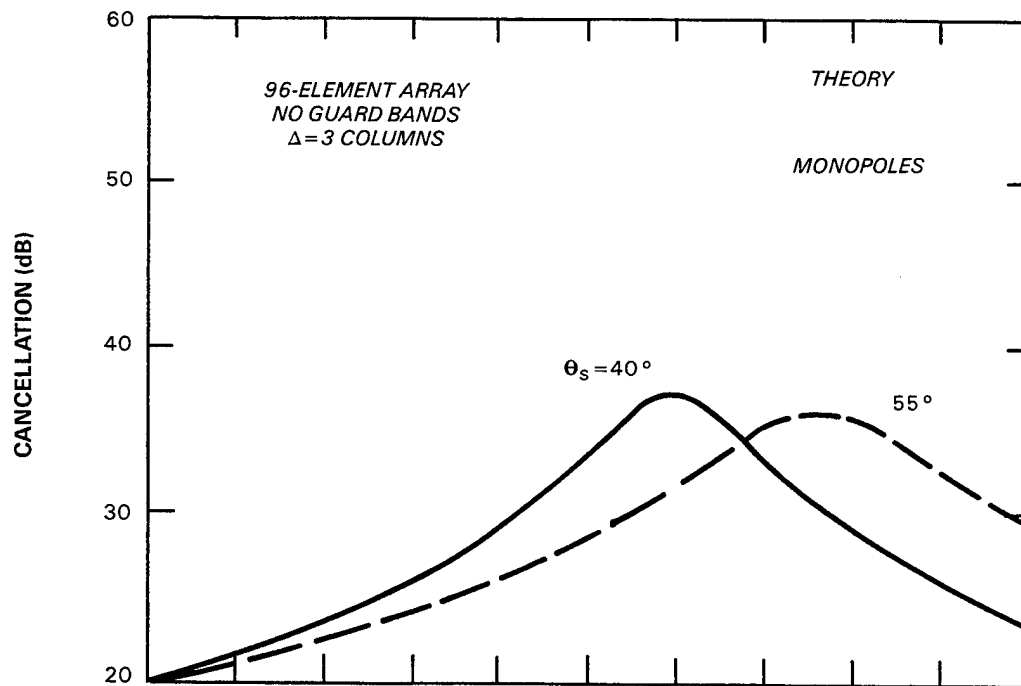
of as a tuning parameter, by which the radar PRI is optimized for the given excitations of the receive antennas.

To demonstrate this effect, consider Figures 3-7 and 3-8 which depict cancellation as a function of change in apparent phase center displacement for monopoles and dipoles. The desired phase center displacement was chosen to be three columns ($\Delta_d = 1.65\lambda$) and scan angles of 40° and 55° were examined. Figure 3-7 is for the case where there are no guard bands and Figure 3-8 is for two guard bands. Notice that the phase center displacement difference Δ_x (in wavelengths) is larger when there are no guard bands. For example, the difference is as large as 0.125λ for the 55° scan angle with monopoles. For the same case but now with two guard bands (Figure 3-8(a)) the displacement difference is only -0.025λ . Thus, one important feature of the guard bands is to stabilize the location of the phase center. The other benefit of guard bands is to increase the cancellation capability as is demonstrated in Figure 3-9. Here, the number of guard bands was varied from zero to four. The improvement in performance is greater than 10 dB for the 40° scan case when two or more guard bands are used compared to zero guard bands. It is interesting to note that the cancellation does not improve substantially (only a few decibels) for the 55° scan with monopoles. The reason for this is not yet explained. In all subsequent performance results shown in this report, it has been assumed that the PRI is matched to the geometrical phase center spacing of the antennas. In those cases (the majority) where guard bands are present, this value is very close to the optimum choice. In the others, it may be assumed that performance could be improved somewhat by a suitable adjustment of the PRI.

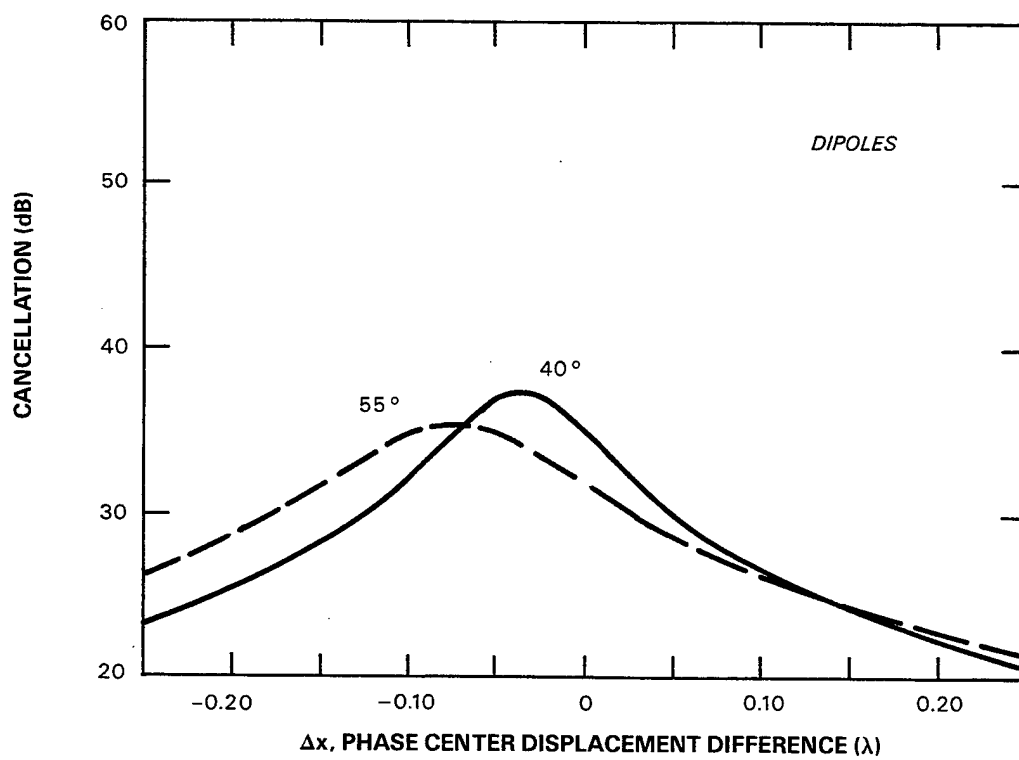
3.3 SUB-SCALE SBR 32-ELEMENT LINEAR PHASED ARRAY

A precision 32-element linear phased array antenna has been constructed for purposes of developing and evaluating ground testing concepts for SBR performance verification [14]. The array operates at L-band and consists of monopole antenna elements arranged in 5 rows and 36 columns. Two rows of passively terminated elements completely surround the center row of 32 active elements. The array elements are arranged in a square lattice with spacing equal to 4.3 inches. The length and diameter of the monopole elements are 2.4 inches and 0.125 inches, respectively. Measurements of the antenna radiation pattern performance (single phase center only) of the 32-element array have been documented [14]. It is planned, at a future date, to measure the DPCA clutter cancellation capability of the array.

A sketch of the corresponding theoretical monopole array over infinite ground plane is shown in Figure 3-10. The shaded center row elements form the 32-element linear array. As in the previous section, dipoles are also theoretically examined. The dipole half-length is chosen to be 2.1 inches, the wire diameter is 0.125 inches, and spacing from the ground plane is 2.1 inches. Each dipole is oriented in the \hat{x} direction.



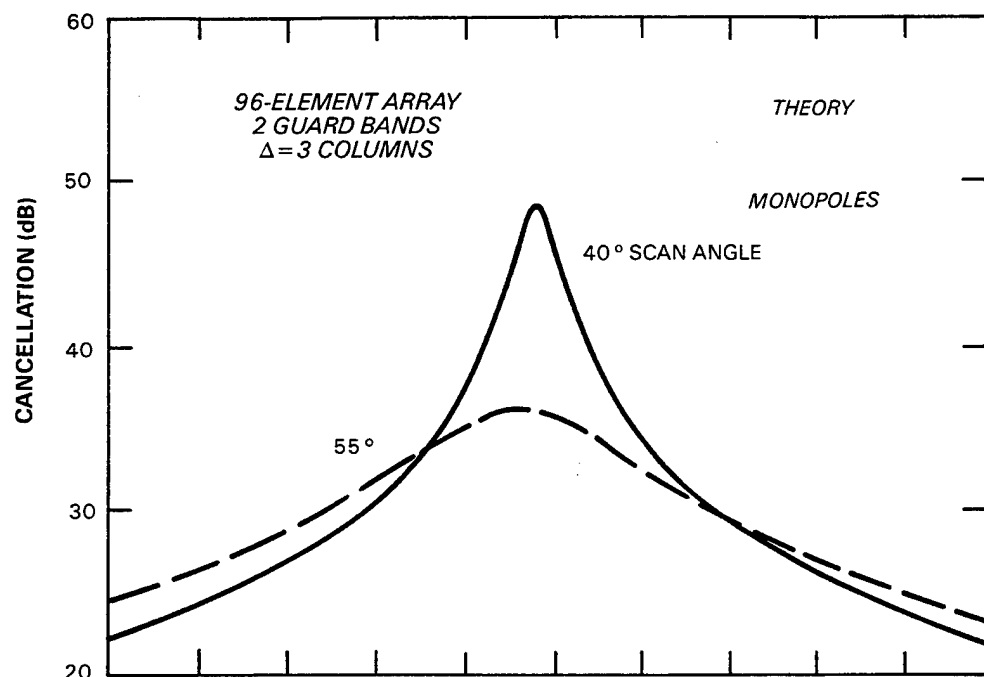
(a)



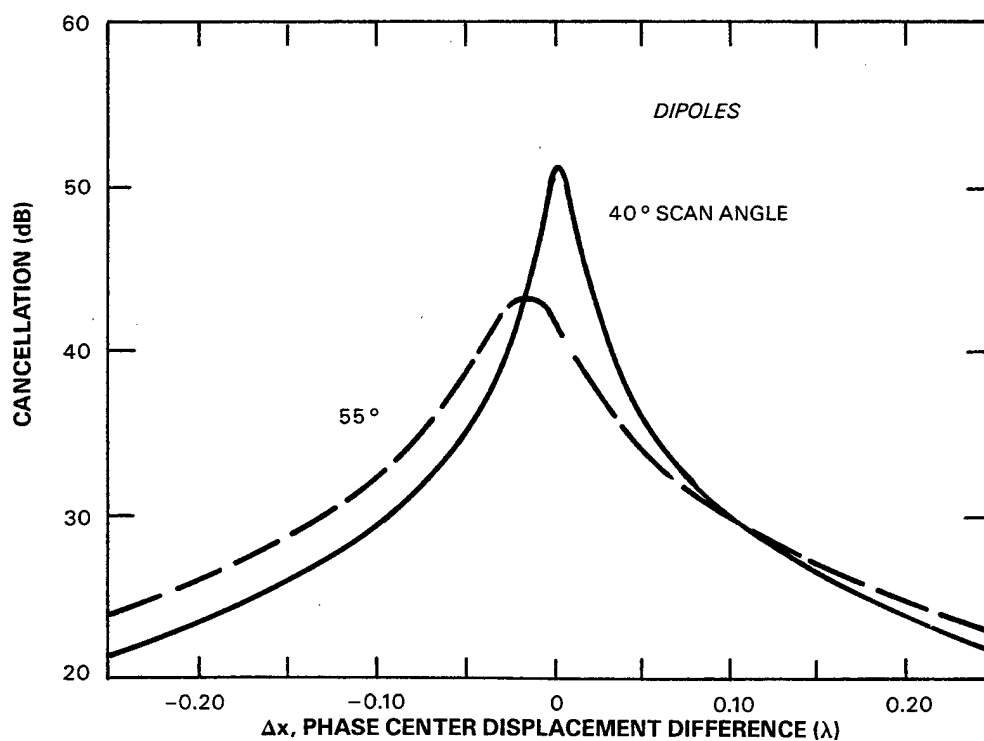
(b)

Figure 3-7. Cancellation versus phase center displacement difference (with no guard bands) for the 96-element test array. (a) monopole elements and (b) dipole elements.

128883-10

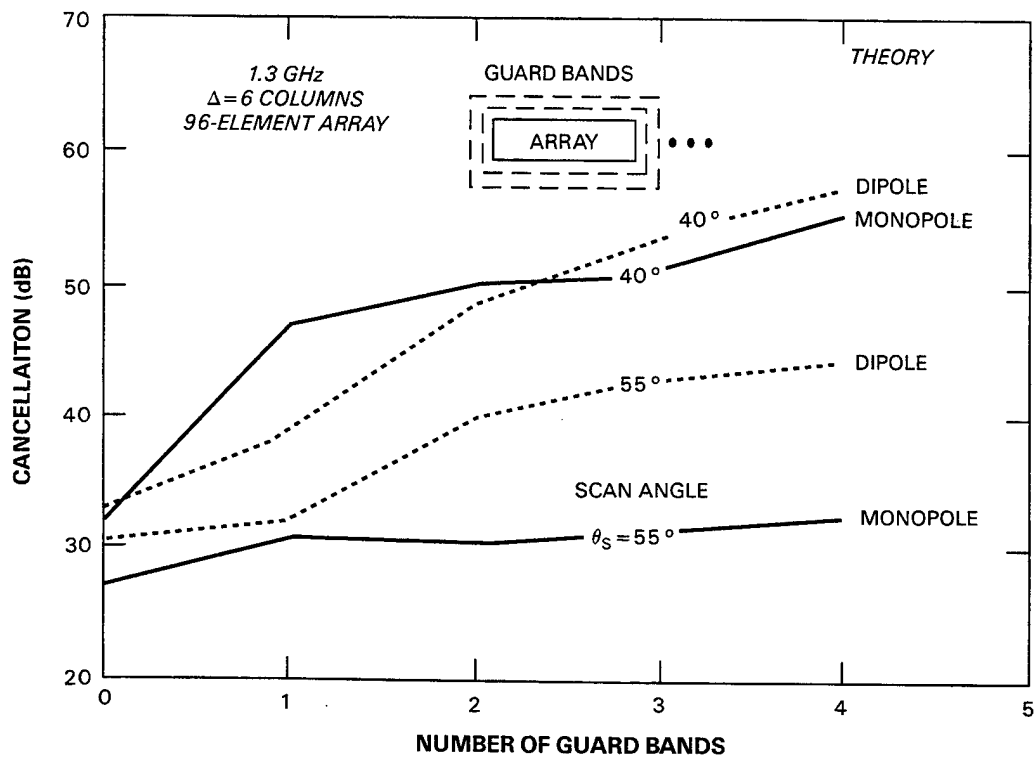


(a)



(b)

Figure 3-8. Cancellation versus phase center displacement difference (with two guard bands) for the 96-element test array. (a) monopole elements and (b) dipole elements.



128883-27

Figure 3-9. Cancellation versus number of guard bands for the 96-element DPCA array.

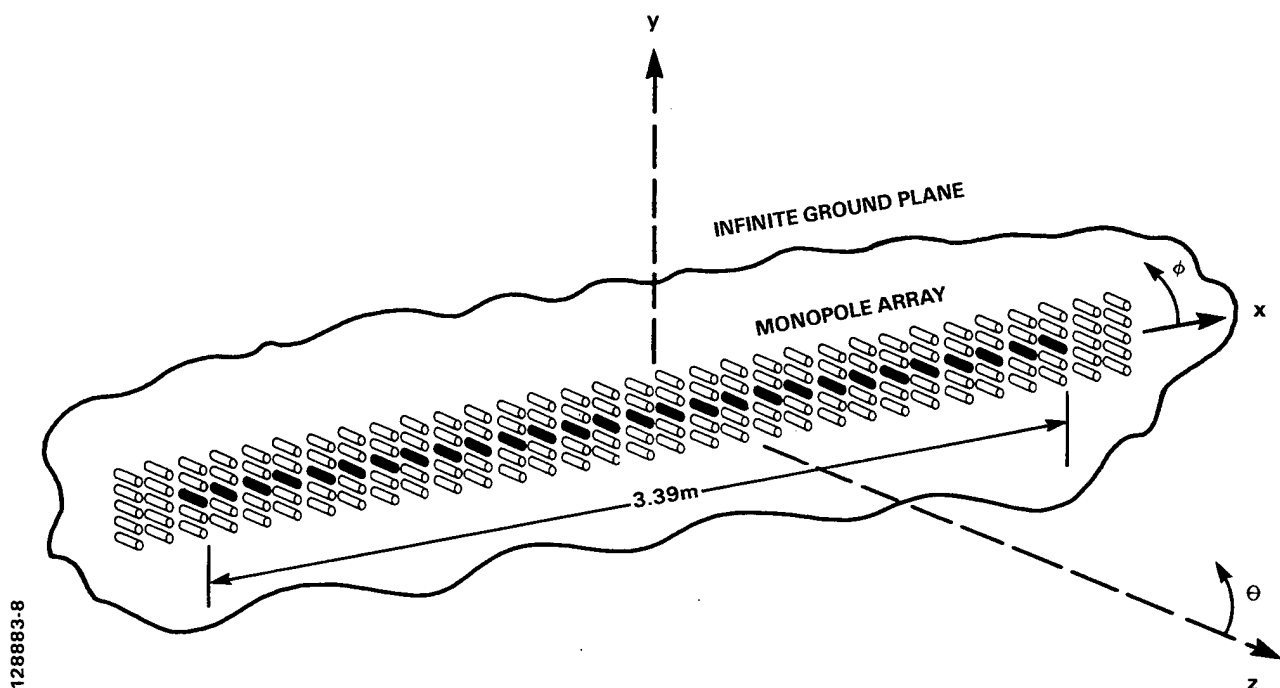
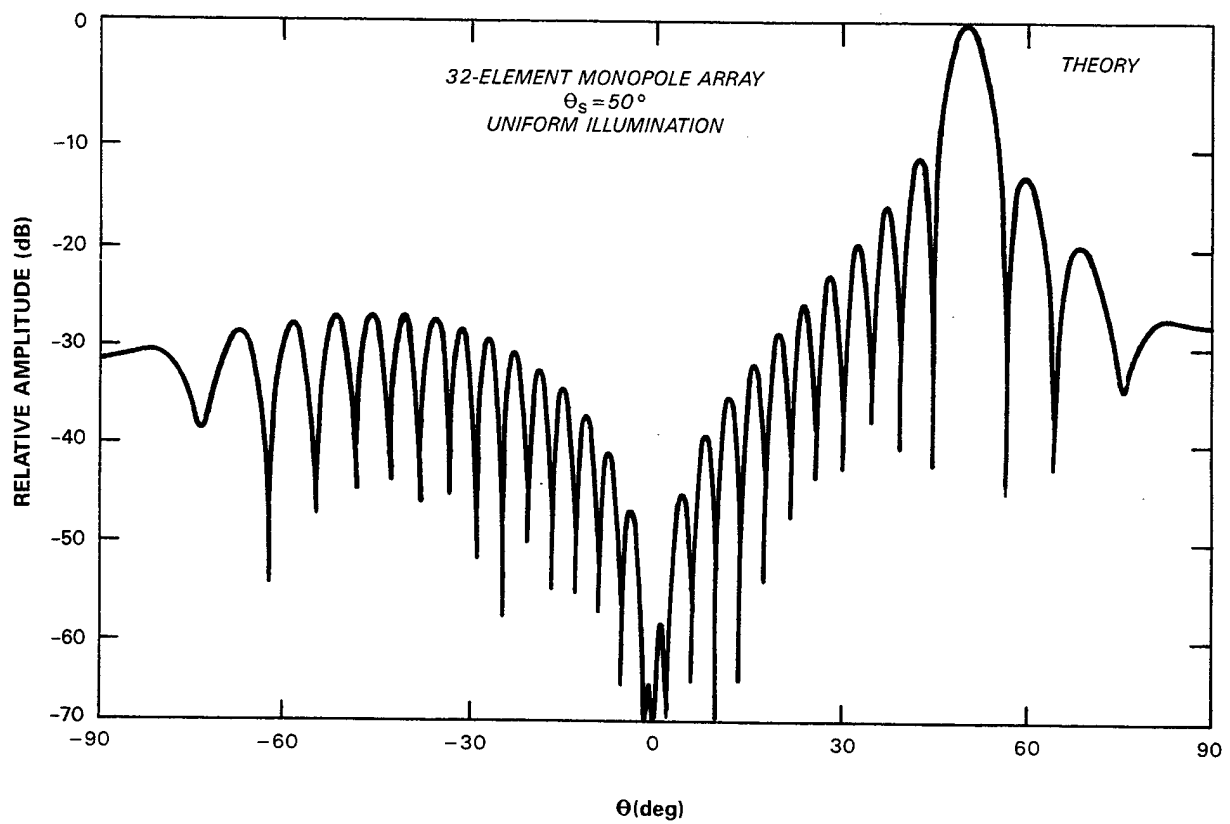


Figure 3-10. Sub-scale SBR 32-element linear test array with monopole elements. Thirty-two elements in the center row are used to form the transmit/receive patterns. Two guard bands of passively terminated elements surround the 32-element linear array.

Predicted radiation patterns for a $\theta = 50^\circ$ scan angle with monopole elements are shown in Figures 3-11 and 3-12. Figure 3-11 is a transmit radiation pattern using uniform illumination across the full aperture. Figure 3-12(a,b) shows the receive radiation patterns using a 40 dB Taylor taper and 8-column phase center displacement.

Consider now, Figure 3-13 which shows cancellation plotted as a function of phase center displacement for various scan angles ($\theta_s \leq 55^\circ$). The array illumination for this case is assumed to be uniform on transmit and 40 dB Taylor on receive. As was observed in the previous section for the 96-element array, the cancellation degrades as the phase center displacement increases. However, for this array lattice (square) and array size the cancellation for monopoles is significantly better than for dipoles. This is the opposite of the



128883-6

Figure 3-11. Transmit radiation pattern using uniform illumination for the 32-element monopole test array. Scan angle is $\theta = 50^\circ$.

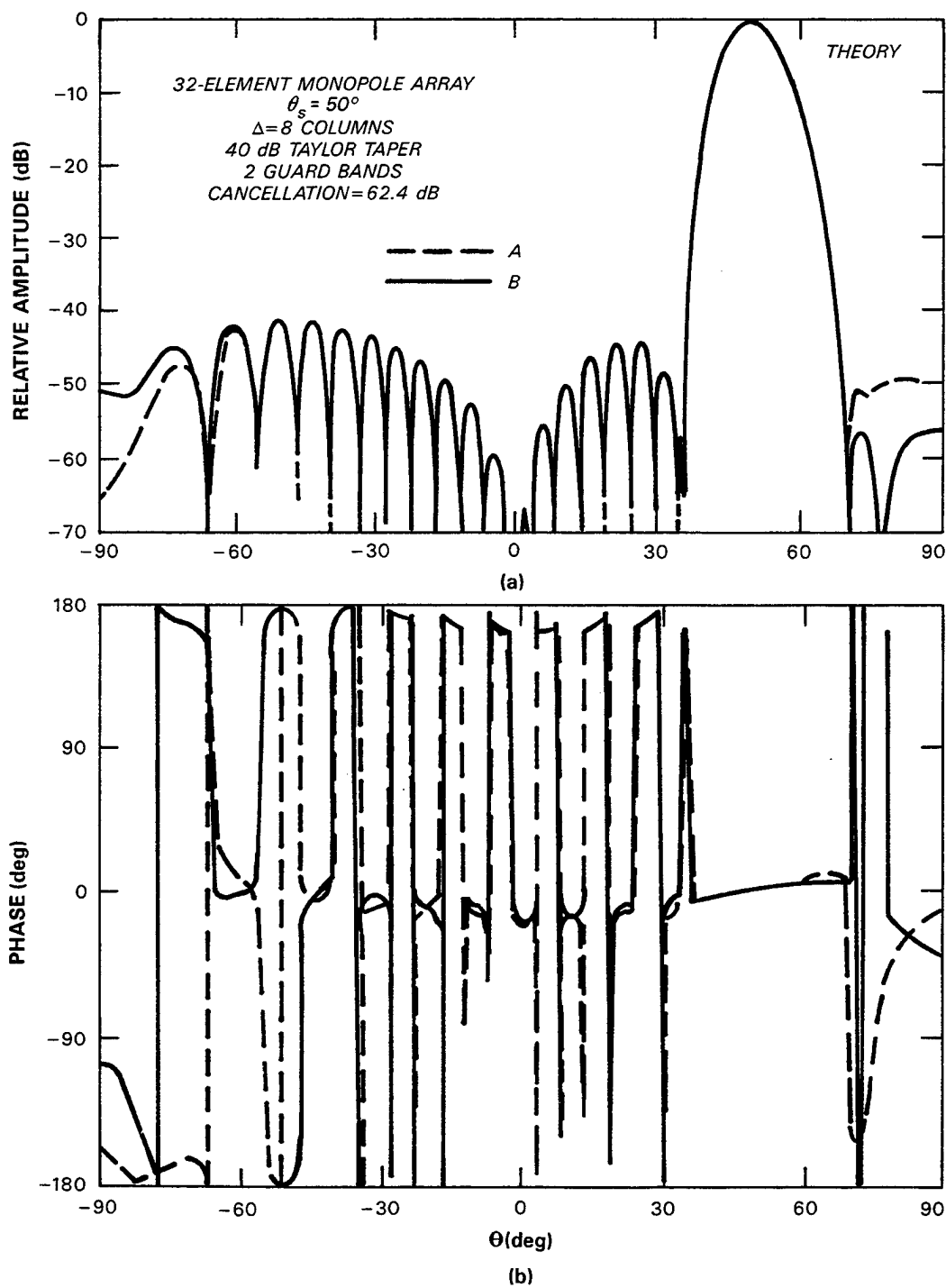


Figure 3-12. Receive array radiation patterns using -40 dB Taylor taper for the 32-element monopole test array. Phase center separation is eight columns. Scan angle is $\theta = 50^\circ$. (a) amplitude and (b) phase.

results obtained for the 96-element array for which it was observed that dipoles performed better than monopoles. The effect of array size and lattice is examined in more detail in the next section.

Next, consider Figure 3-14 which shows cancellation as a function of scan angle for 32-element arrays of monopole and dipole elements. Calculations are shown for 8- and 16-column phase center displacements and for two types of array illumination. The solid curves are for uniform transmit illumination and 40 dB Taylor taper on receive, and the dashed curves are for -10 dB cosine taper on transmit and receive. Note that the choice of taper does affect the results. The effect of taper appears to be less significant for dipoles compared to monopoles. In Figure 3-15(a) for the case of uniform transmit/40 dB Taylor receive illumination, the effect of element type is depicted. Similarly, in Figure 3-15(b) (10 dB cosine taper transmit/receive) monopoles and dipoles are compared.

The effect of number of guard bands is depicted in Figure 3-16. The number of guard bands was varied from one to four and it is clear that increasing the number of guard bands from one to two can improve the clutter cancellation. However, as this figure shows, increasing the guard bands beyond two does not necessarily improve performance (observe the 40° dipole case).

3.4 SUB-SCALE AND FULL-SCALE SBR PLANAR PHASED ARRAYS

The previous sections have dealt with specific phased array antenna designs - a 96-element planar array and a 32-element linear array. In this section, the effect of the array size on DPCA performance will be investigated. Array sizes up to 16 meters are considered. The designation sub-scale array will be used arbitrarily to refer to antennas less than 12 meters in length. Of primary interest is the effect of array length along the dimension of phase center displacement. The number of active rows is fixed at eight, and the number of active columns is made variable, as depicted in Figure 3-17. With eight active rows and two guard bands, for a 16-meter aperture there are a total of 148 columns by 12 rows (1776 unknowns) in the square lattice case. For the same aperture size, with a hexagonal lattice, the number of columns is 132 and the number of rows is 12 (1584 unknowns). Both monopole and dipole radiators are evaluated here. A low-altitude SBR system is assumed as in the previous sections. The array element spacing is selected to provide $\pm 60^\circ$ coverage. At center frequency, 1.3 GHz, with a square lattice the element spacing is 0.473λ and with a hexagonal lattice the spacing is 0.55λ . The monopole length is 2.5 inches for the square lattice and 2.3 inches for the hexagonal lattice. The dipole half-length is 2.1 inches in the square lattice and 2.2 inches in the hexagonal lattice. The dipole spacing over ground plane is 2.1 inches.

Consider Figure 3-18(a) which shows the cancellation as a function of number of active columns for a square lattice. Here, the number of active columns has been varied from

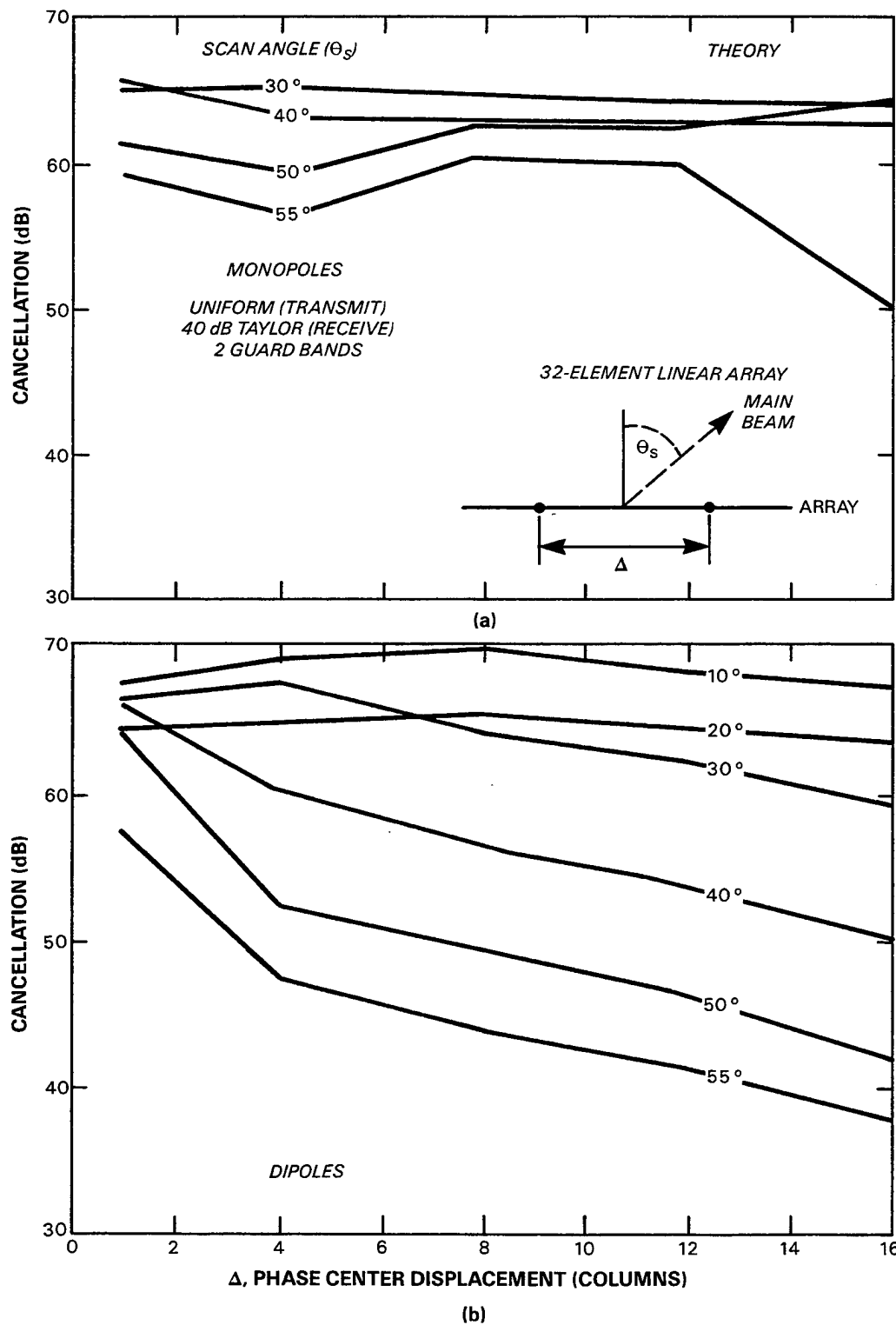


Figure 3-13. Cancellation as a function of phase center displacement in columns for the 32-element test array. (a) monopole elements and (b) dipole elements.

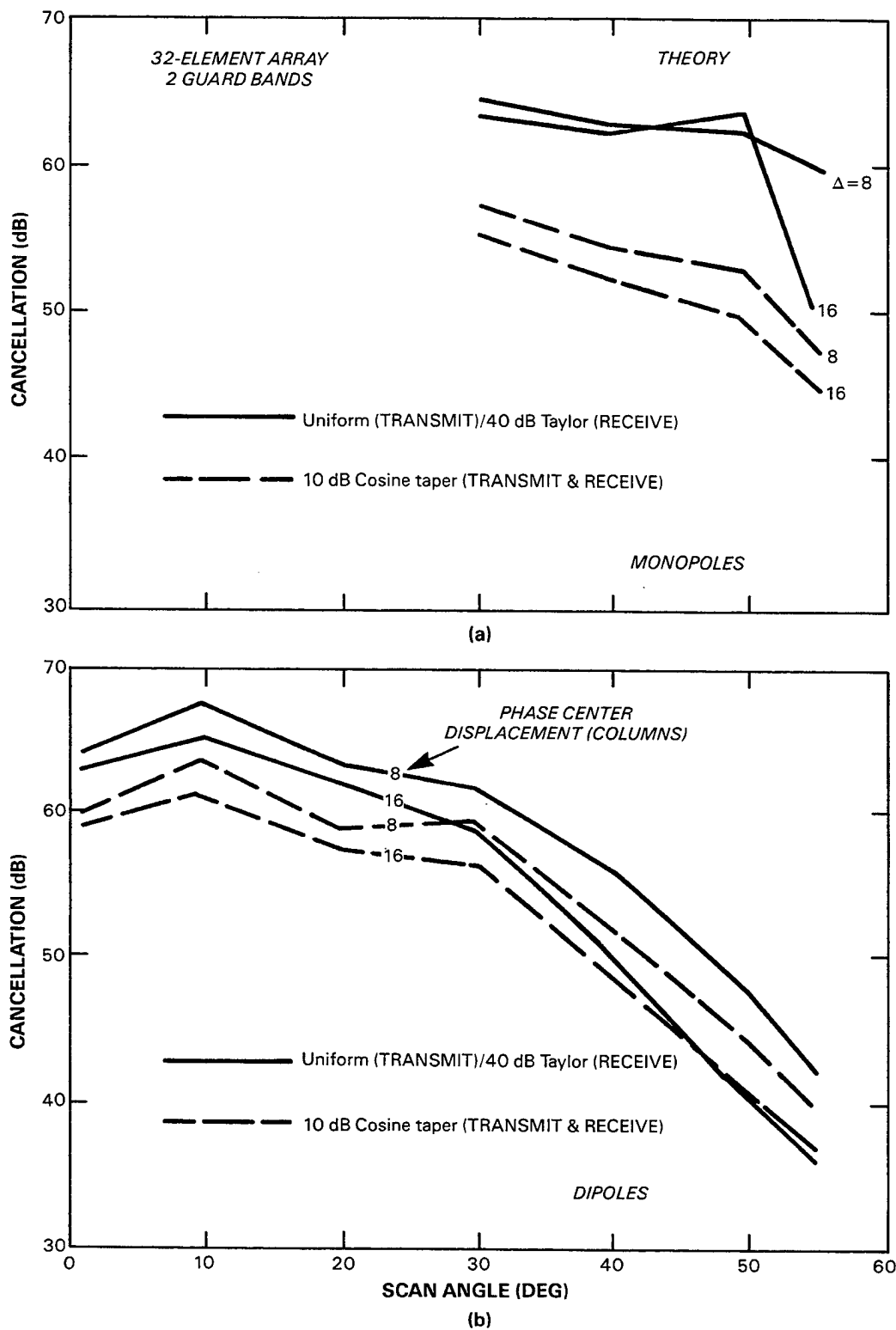


Figure 3-14. Cancellation as a function of scan angle using different array illuminations with 8- and 16-column phase center separation for the 32-element test array. (a) monopole elements and (b) dipole elements.

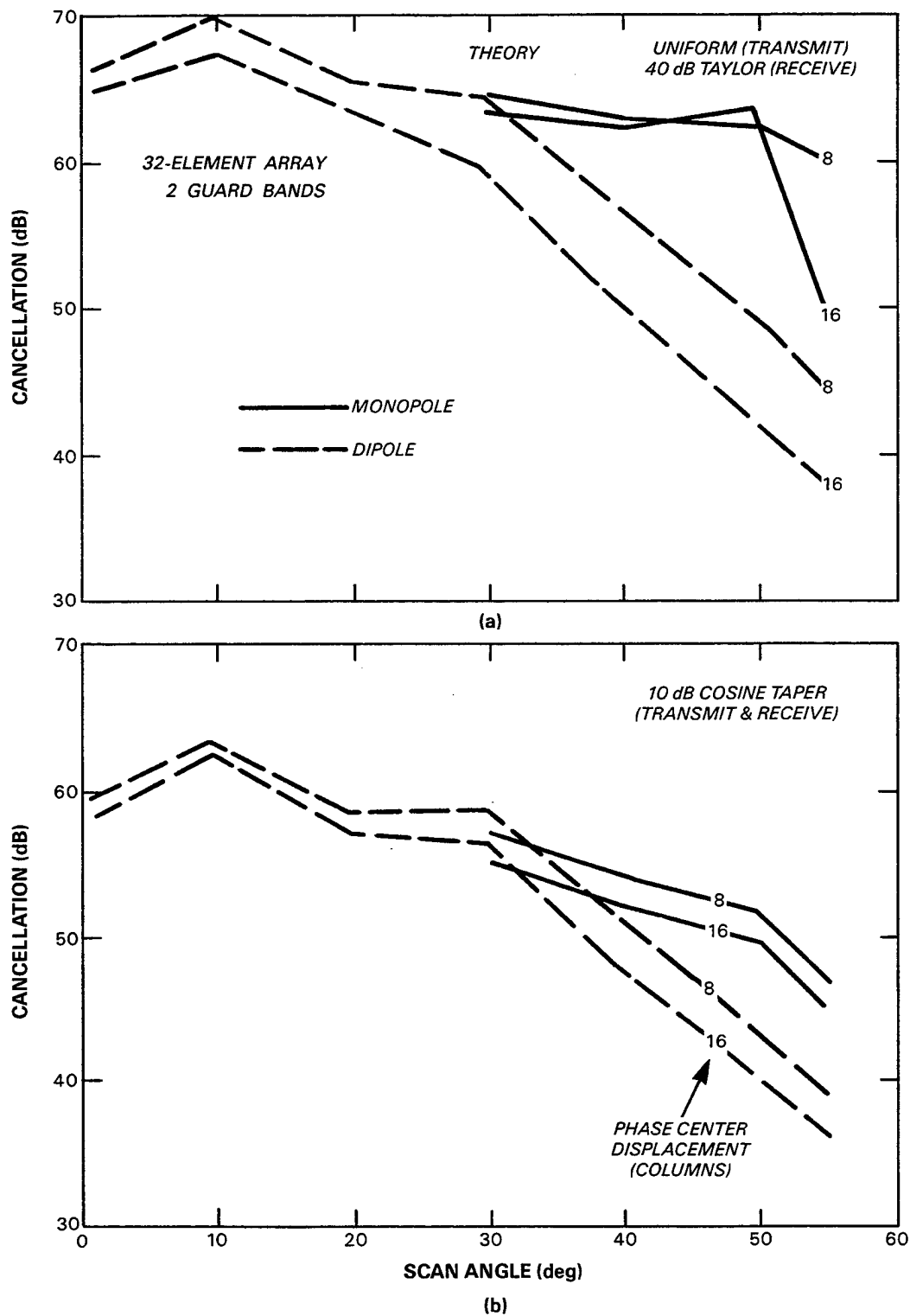
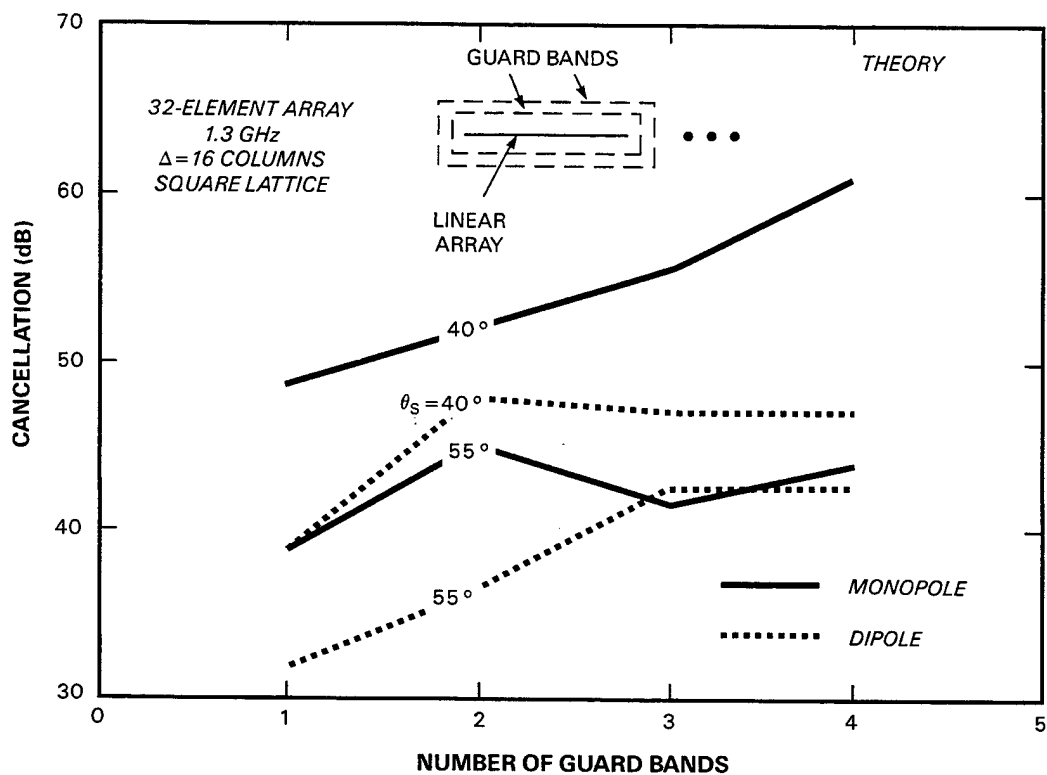


Figure 3-15. Cancellation as a function of scan angle using monopole and dipole array elements with 8- and 16-column phase center separation for the 32-element test array. (a) uniform transmit illumination/40 dB Taylor receive illumination and (b) cosine transmit/receive illumination with 10 dB edge taper.



128883-26

Figure 3-16. Cancellation versus number of guard bands for the 32-element DPCA array.

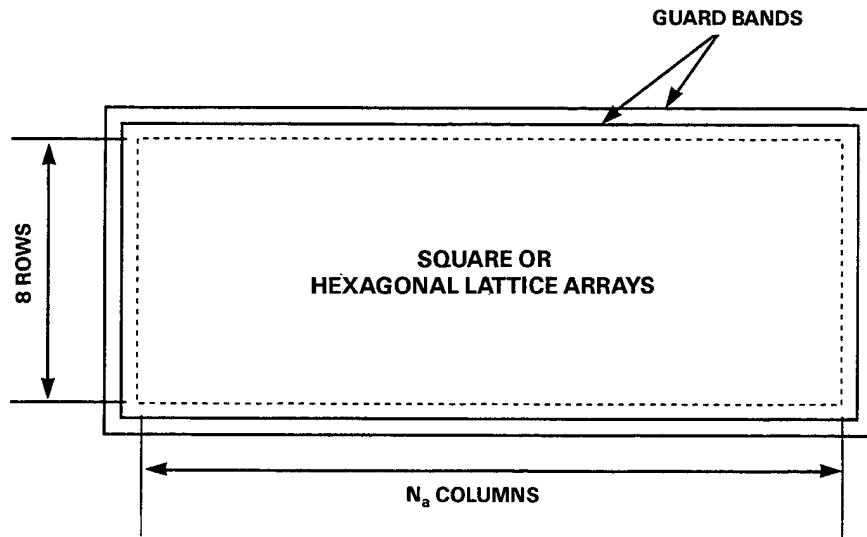


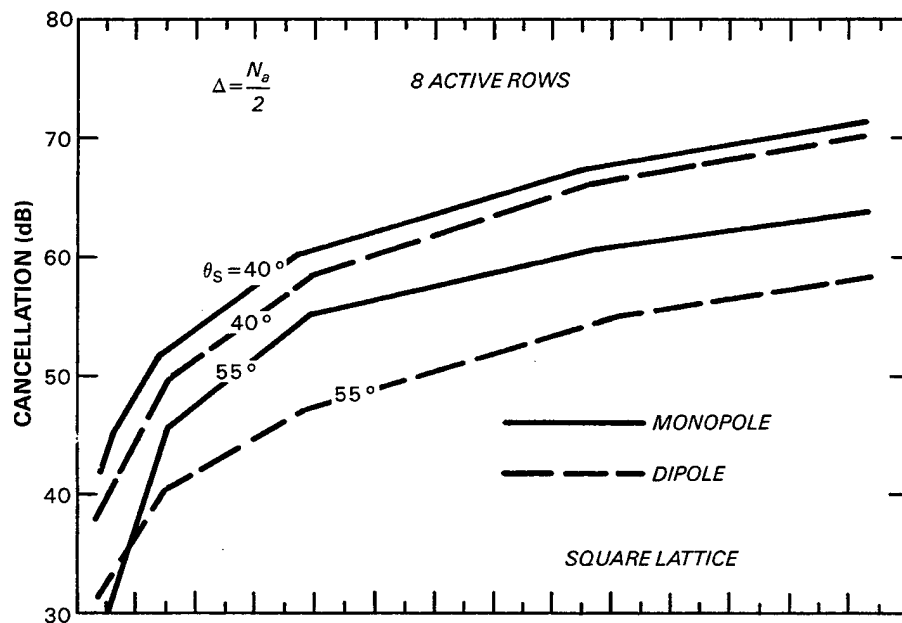
Figure 3-17. Sub-scale and full-scale array geometry. The number of active rows is fixed at eight. The number of active columns is variable. Two guard bands surround the active array.

12 to 144. For the two scan angles shown, it is clear that the monopole offers a slight improvement over dipoles. However, in Figure 3-18(b) (hexagonal lattice) the cancellation is approximately the same for either monopoles or dipoles. Replotting the same results in Figure 3-19(a,b), the effect of the array lattice on cancellation is clearly shown. The effect of the lattice is greater for dipoles than for monopoles. In Figure 3-20(a,b) the same results are again replotted, this time as a function of array length in meters. From these data it is observed that, for arrays greater than 4 meters, the cancellation increases typically by 8 dB when the array length increases by a factor of two. It should be noted that the cancellation shown here does not include the effects of element weighting errors. That is, the high values of cancellation may not actually be achieved in practice. The cancellation will be limited by the random errors produced by the transmit/receive modules.

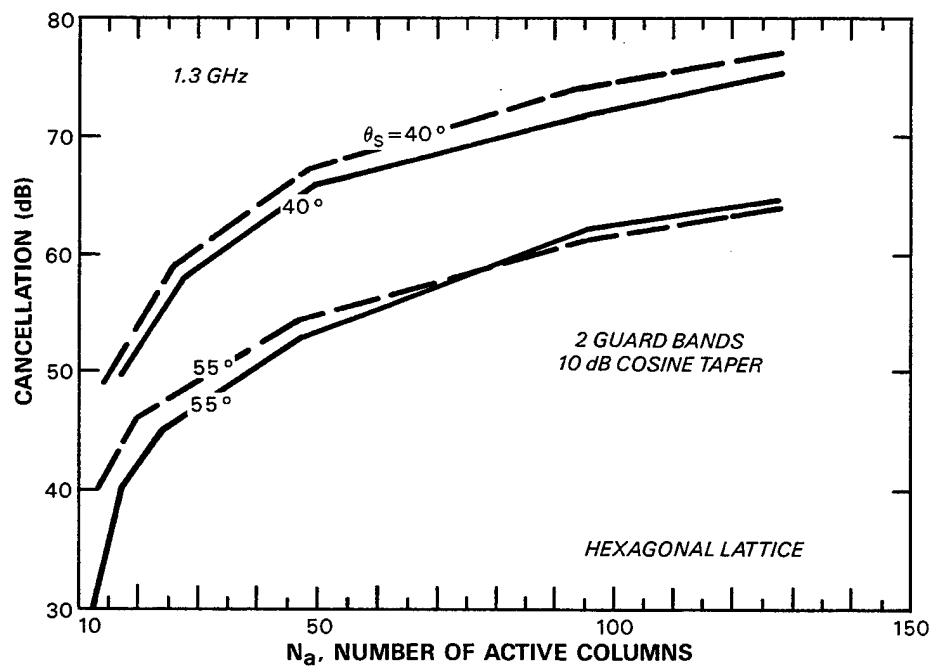
Now, consider the effect of varying the phase center displacement for a fixed size array consisting of 8 active rows and 128 active columns. The array lattice is assumed to be hexagonal and there are two guard bands. Two scan angles were considered for monopoles and dipoles and the phase center displacement was varied from 8 to 64 columns. The results are shown in Figure 3-21 where it is observed that the cancellation is insensitive to phase center displacement.

To show that the above results do not depend on the number of active rows, the number of columns was fixed at 128 and the number of active rows was varied from 4 to 16. The array lattice is hexagonal and there are two guard bands. The phase center displacement was assumed to be 64 columns. Figure 3-22 clearly shows that there is little change in the clutter cancellation as the number of active rows is varied.

Finally, the effect of number of guard bands for an 8 active row by 128 active column array is shown in Figure 3-23. As has been observed in the previous sections, two guard bands provide higher cancellation than no guard bands.



(a)



(b)

Figure 3-18. Cancellation as a function of number of active array columns for one-half aperture phase center spacing using monopole and dipole antenna elements. (a) square lattice and (b) hexagonal lattice.

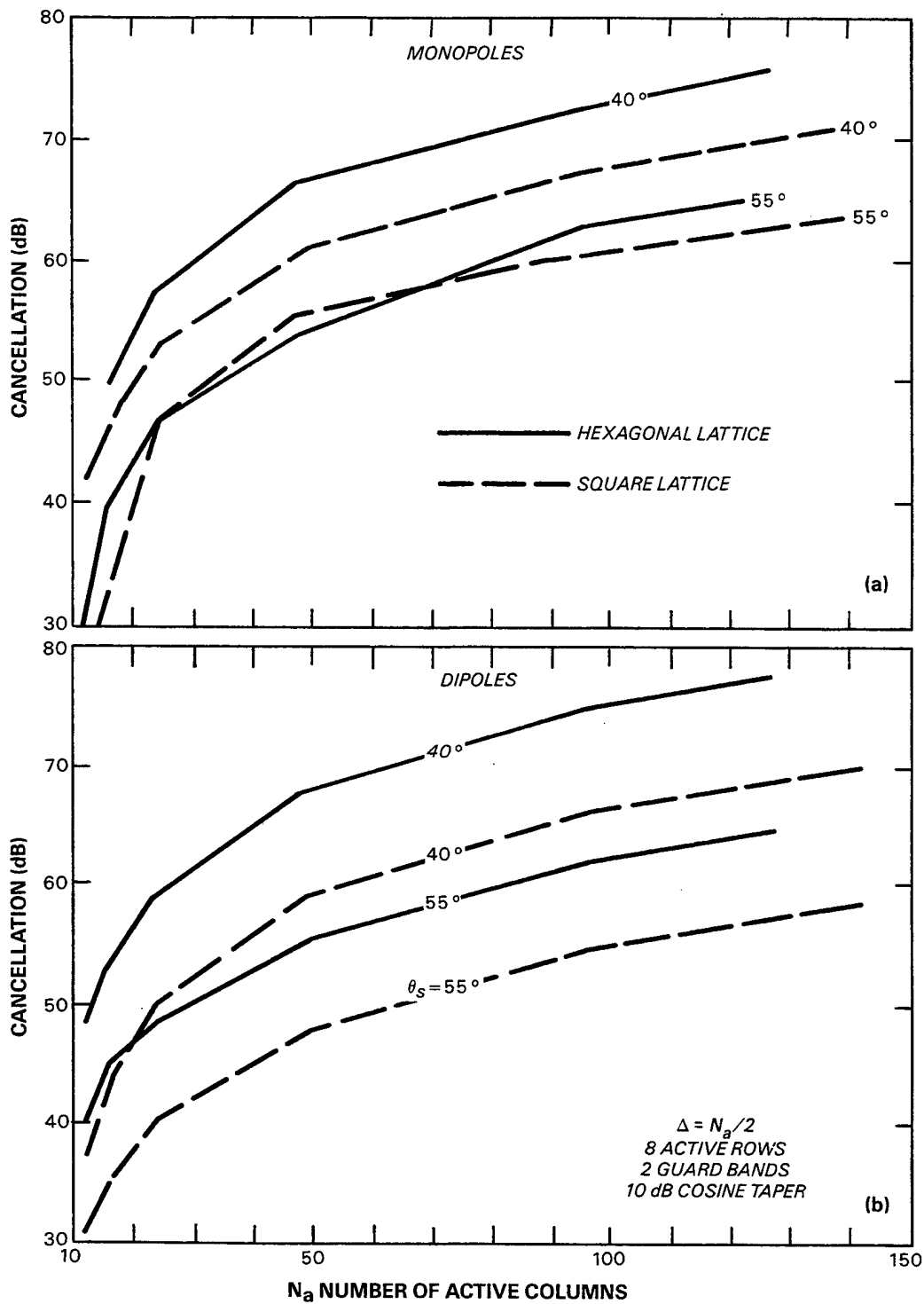


Figure 3-19. Cancellation as a function of number of active array columns for one-half aperture phase center spacing using square and hexagonal array lattices. (a) monopole elements and (b) dipole elements.

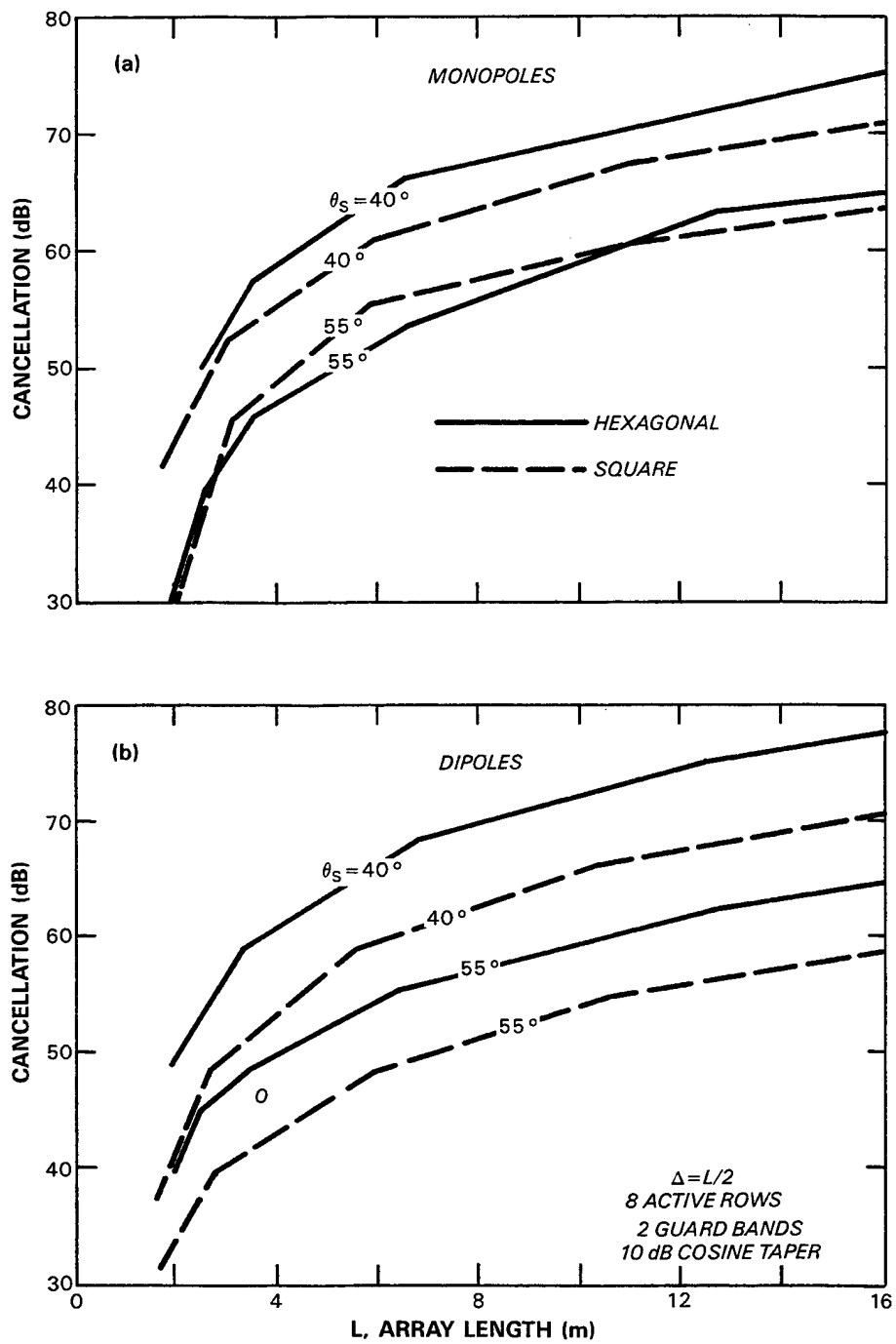


Figure 3-20. Cancellation as a function of array length for one-half aperture phase center spacing using square and hexagonal array lattices. (a) monopole elements and (b) dipole elements.

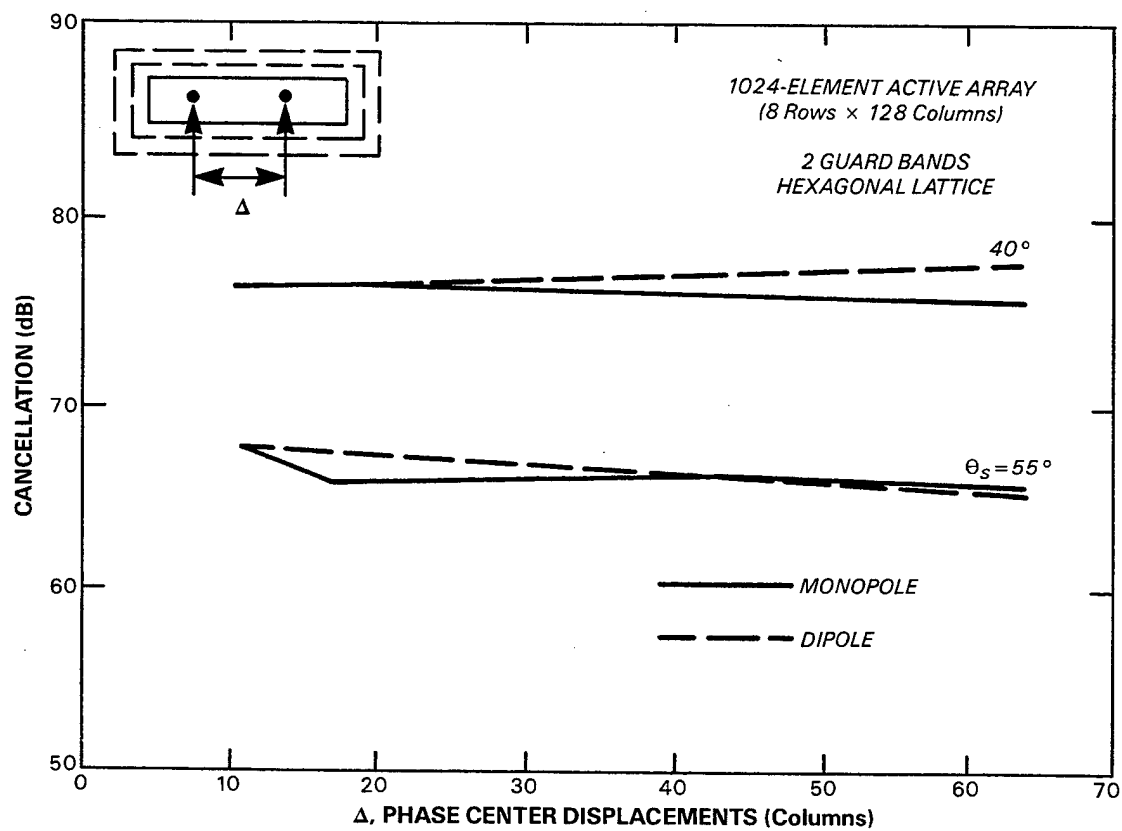


Figure 3-21. Cancellation versus phase center displacement in columns for an 8 active row by 128 active column DPCA array.

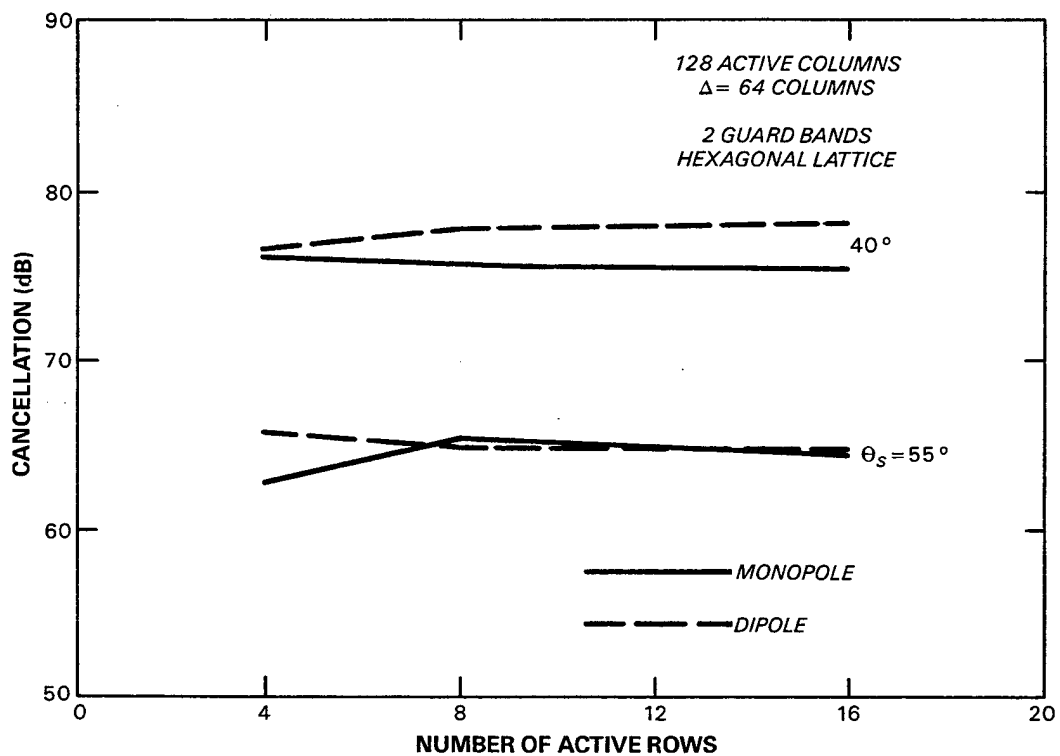
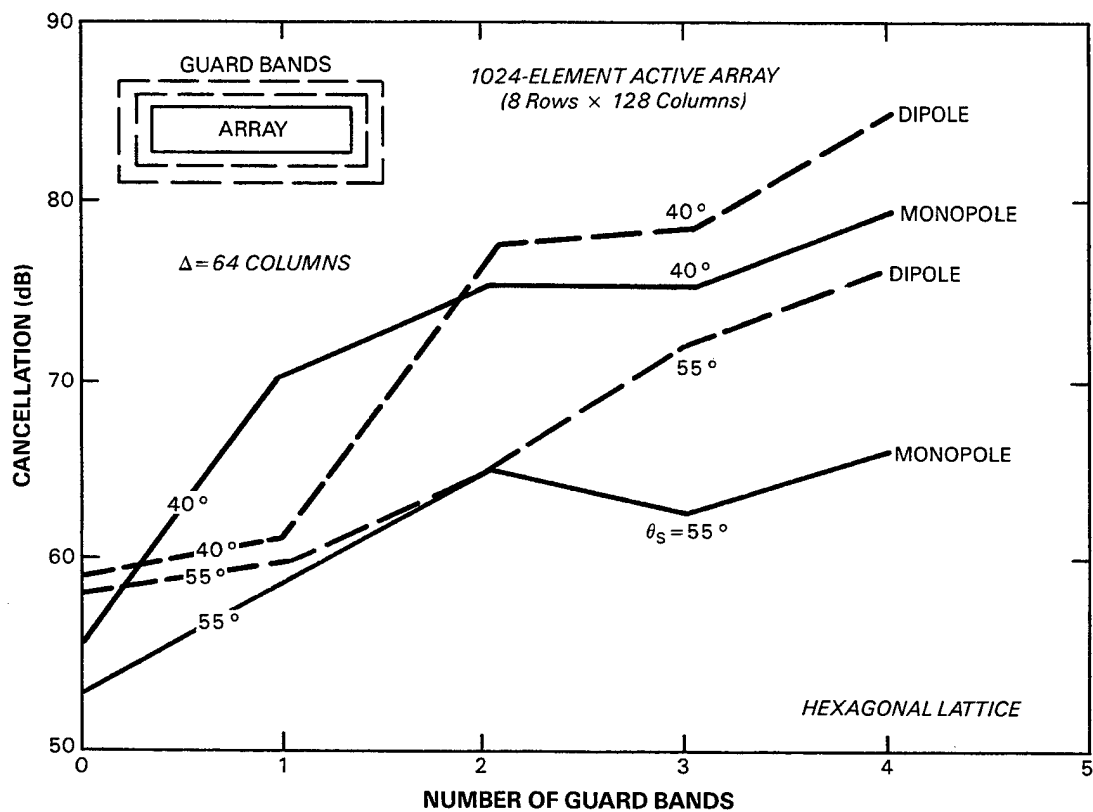


Figure 3-22. Cancellation versus number of active rows in an array having 128 active columns.



128883-29

Figure 3-23. Cancellation versus number of guard bands for an 8 active row by 128 active column DPCA array.

4. CONCLUSION

This report has investigated the subject of array mutual coupling effects on the displaced phase center antenna (DPCA) clutter cancellation capability of corporate-fed phased array antennas. Mutual coupling effects have been modeled using the method of moments for monopole and dipole phased array antennas. Finite array edge effects and polarization are inherently included in the analysis. The assumption of an infinite ground plane was made in the theoretical formulation. The effects of transmit/receive module random errors have been ignored in this analysis. The theoretical results presented are the upper-bound clutter cancellation limited by mutual coupling alone.

In Section 2 the theoretical formulation was discussed. A derivation of the factor used to quantify clutter cancellation has been given in Appendix A.

A variety of sub-scale and full-scale SBR antennas have been analyzed in Section 3. One such array was a 96-element planar array of monopoles for which measured DPCA clutter cancellation capability data was available. The theoretical calculations were shown to be consistent with measurements. Another sub-scale array investigated was a 32-element linear array which corresponds to a DPCA antenna that has been constructed and is planned to be tested. These tests will be particularly important in validating the theoretical simulation. For this antenna, DPCA clutter cancellation predictions have been made and will be compared with experiments when the measured data become available. Finally, planar arrays of various sizes, corresponding to sub-scale and full-scale SBR antennas have been analyzed.

Based on the results presented in this report, it is clear that general statements about the effect of varying the DPCA design parameters are difficult to make. It has been shown that the clutter cancellation capability of an array is sensitive to many parameters. These include the scan angle, array illumination, phase center displacement, array size, array lattice, number of passively terminated element guard bands, and radiating element type. Some conclusions which can be made are: The cancellation tends to increase as the array size or number of guard bands increases. For large arrays (>12 meters), a hexagonal lattice provides better cancellation than does a square lattice. For smaller arrays, the best cancellation which can be achieved for a given lattice depends on the array element. The array element type strongly affects the amount of clutter cancellation achieved in sub-scale arrays.

More work is needed to fully understand how the mutual coupling in an array affects DPCA performance. For example, in the present moment method model there is one unknown current function per element of the array. It is desirable to be able to vary the number of unknowns per element of the array to check the convergence of the clutter cancellation. This may lead to improved prediction capability. Also, the effect of transmit/receive module errors could be included in the mutual coupling formulation. This would likely provide a

clutter cancellation prediction capability that would more closely relate to a practical DPCA radar system.

APPENDIX A

DERIVATION OF CLUTTER CANCELLATION FACTOR

Consider an N -channel adaptive nulling processor which uses a quiescent steering weight vector \mathbf{w}_q in the design of an adaptive weight vector \mathbf{w}_a for detection. It is assumed that \mathbf{w}_q is normalized, such that $\mathbf{w}_q^\dagger \mathbf{w}_q = 1$. Let it be assumed at first that the true noise covariance matrix \mathbf{M} is known and that it consists of receiver noise and clutter. Let the N -channel output vector prior to weighting be denoted \mathbf{x} . For a given weight vector \mathbf{w} , the weighted output is expressed as

$$y = \mathbf{w}^\dagger \mathbf{x}. \quad (\text{A.1})$$

Detection will be based on the magnitude of the adaptively weighted quantity

$$y_a = \mathbf{w}_a^\dagger \mathbf{x} \quad (\text{A.2})$$

where,

$$\mathbf{w}_a = \mathbf{M}^{-1} \mathbf{w}_q. \quad (\text{A.3})$$

Now, let \mathbf{s} denote the desired signal (target) vector and let \mathbf{n} be the noise-only channel vector. It is assumed that $\mathbf{E}(\mathbf{n}\mathbf{n}^\dagger) = \mathbf{M}$ and $\mathbf{E}(\mathbf{n}) = 0$, where \mathbf{E} means mathematical expectation. The desired signal vector can be written as

$$\mathbf{s} = A\mathbf{p} \quad (\text{A.4})$$

where A is a complex amplitude parameter and \mathbf{p} is a normalized vector which contains the relative signal phase shift between channels. It follows that the desired signal expected value or mean is $\mathbf{E}(\mathbf{s}) = A\mathbf{p}$.

The channel output vector is equal to the superposition of signal and noise as,

$$\mathbf{x} = \mathbf{s} + \mathbf{n}. \quad (\text{A.5})$$

From the above it is clear that the expected value of the signal plus noise vector is given by

$$\mathbf{E}_{\mathbf{s}+\mathbf{n}}(\mathbf{x}) = A\mathbf{p}. \quad (\text{A.6})$$

The signal-to-noise ratio (SNR) is defined as the ratio of the output power of the signal alone to the output power of the noise alone. It follows then that the weighted channel output signal-to-noise ratio can be expressed as

$$SNR \equiv \frac{|\mathbf{E}_{s+n}(y) - \mathbf{E}_n(y)|^2}{\mathbf{E}_n|y|^2}. \quad (\text{A.7})$$

Now, in Equation (A.7) $\mathbf{E}_n(y) = 0$ and

$$\mathbf{E}_{s+n}(y) = \mathbf{w}^\dagger \mathbf{E}_{s+n}(\mathbf{x}) \quad (\text{A.8})$$

where the weight vector \mathbf{w} is equal to either \mathbf{w}_q before adaption or \mathbf{w}_a after adaption. Before adaption, the expected value of y_q for signal plus noise is

$$\mathbf{E}_{s+n}(y_q) = A\mathbf{w}_q^\dagger \mathbf{p}. \quad (\text{A.9})$$

The quiescent output power due to noise is expressed as

$$\mathbf{E}_n|y_q|^2 = \mathbf{w}_q^\dagger \mathbf{M} \mathbf{w}_q. \quad (\text{A.10})$$

Substituting Equations (A.9) and (A.10) into (A.7) yields, for the quiescent signal-to-noise ratio,

$$SNR_q = |A|^2 \frac{|\mathbf{w}_q^\dagger \mathbf{p}|^2}{\mathbf{w}_q^\dagger \mathbf{M} \mathbf{w}_q}. \quad (\text{A.11})$$

To find the adapted SNR, first substitute Equations (A.3) and (A.6) in (A.8) which produces

$$\mathbf{E}_{s+n}(y_a) = A\mathbf{w}_q^\dagger \mathbf{M}^{-1} \mathbf{p}. \quad (\text{A.12})$$

Next, the output power due to clutter and receiver noise is given by

$$\mathbf{E}_n|y_a|^2 = \mathbf{w}_a^\dagger \mathbf{M} \mathbf{w}_a. \quad (\text{A.13})$$

Substituting Equation (A.3) in (A.13) yields

$$\mathbf{E}_n|y_a|^2 = \mathbf{w}_q^\dagger \mathbf{M}^{-1} \mathbf{w}_q. \quad (\text{A.14})$$

Equations (A.12) and (A.14) are substituted into Equation (A.7) with the result

$$SNR_a = |A|^2 \frac{|\mathbf{w}_q^\dagger \mathbf{M}^{-1} \mathbf{p}|^2}{\mathbf{w}_q^\dagger \mathbf{M}^{-1} \mathbf{w}_q}. \quad (\text{A.15})$$

In practice, the covariance matrix is not known, and is usually estimated from some set of sample vectors which have the same noise statistics as \mathbf{x} , but which are free of signal components. This estimation procedure causes a loss in output SNR which was first studied by Reed, Mallet, and Brennan [15] for the matched case in which $\mathbf{p} = \mathbf{w}_q$, and by Boroson [16] for the general mismatched case. In either case, if the covariance estimate is based on a sufficiently large number of samples, the loss in SNR is small, and it will be ignored in the remainder of this discussion.

In the two-phase center DPCA case, there are only two channels ($N = 2$), and a typical signal vector has form $\mathbf{s} = A\mathbf{p}$, where

$$\mathbf{p} = \frac{1}{\sqrt{2}} \begin{bmatrix} 1 \\ e^{i\psi} \end{bmatrix}. \quad (\text{A.16})$$

This is a normalized vector, and the phase angle ψ corresponds to the Doppler shift associated with the range rate of the target itself. Let the covariance matrix of the clutter-plus-receiver noise output of the two channels be

$$\mathbf{M} = \begin{bmatrix} M_{11} & M_{12} \\ M_{21} & M_{22} \end{bmatrix}. \quad (\text{A.17})$$

Instead of steering for a variety of values of ψ , it has been found to be sufficient to use a single "mismatched" steering vector,

$$\mathbf{w}_q \equiv \begin{bmatrix} 1 \\ 0 \end{bmatrix}. \quad (\text{A.18})$$

Substituting Equations (A.16), (A.17), and (A.18) into (A.11) yields

$$\text{SNR}_q = \frac{|A|^2}{2M_{11}} \quad (\text{A.19})$$

which is the SNR for channel 1 alone. The clutter returns will usually dominate the noise, and since they will have very nearly the same power in the two channels (if the latter are well matched) then the SNR in channel 2 will be essentially the same as that of channel 1.

Next, to compute the adapted SNR, the inverse of \mathbf{M} is needed and is simply

$$\mathbf{M}^{-1} = \frac{1}{\Delta} \begin{bmatrix} M_{22} & -M_{12} \\ -M_{21} & M_{11} \end{bmatrix} \quad (\text{A.20})$$

where,

$$\Delta = M_{11}M_{22} - M_{12}M_{21} \quad (\text{A.21})$$

is the determinant of \mathbf{M} . Substituting Equations (A.16), (A.18), and (A.20) into (A.15) produces the signal-to-noise ratio after adaption,

$$SNR_a = \frac{|A|^2 |M_{22} - M_{12}e^{i\psi}|^2}{2\Delta M_{22}}. \quad (\text{A.22})$$

This expression can be rewritten in the form

$$SNR_a = \frac{|A|^2}{2CM_{11}} \left| 1 - \frac{M_{12}}{M_{22}} e^{i\psi} \right|^2 \quad (\text{A.23})$$

where C , the clutter cancellation factor, is defined by

$$C \equiv 1 - \frac{|M_{12}|^2}{M_{11}M_{22}}. \quad (\text{A.24})$$

For strong clutter, M_{12} will be very nearly equal to M_{22} , and the factor

$$\left| 1 - \frac{M_{12}}{M_{22}} e^{i\psi} \right|^2 \approx |1 - e^{i\psi}|^2 = 4\sin^2(\psi/2) \quad (\text{A.25})$$

then describes the variation of SNR with true target Doppler. For targets with very small range rates, ψ will be nearly zero, and the output SNR itself will be very small. These are targets which are lost in the clutter return. When $\psi = \pi$, the target range rate corresponds to the "optimum speed," in the terminology of conventional MTI radar, and the second factor in the SNR formula will represent approximately 6 dB of gain. In this case, the target returns from the two phase centers are combining coherently, and the effective gain of the full antenna is restored.

The other factor $|A|^2/(2CM_{11})$ in Equation (A.23) is just like the SNR on channel 1 (Equation (A.19)), but with the clutter-plus-noise power M_{11} reduced by the "cancellation factor" C . This is the quantity in terms of which the DPCA performance is evaluated in the body of this report.

REFERENCES

1. M. L. Stone and W. J. Ince, "Air-to-Ground MTI Radar Using a Displaced Phase Center Phased Array," The Record of the IEEE 1980 International Radar Conference, Arlington, VA, 29-30 April 1980, pp.225-230.
2. M. I. Skolnik, *Introduction to Radar Systems*, 2nd edition, McGraw Hill, 1980, pp. 143-144.
3. E. J. Kelly and G. N. Tsandoulas, "A Displaced Phase Center Antenna Concept for Space-Based Radar Application," *IEEE Eascon*, pp. 141-148, September 1983.
4. R. W. Miller, "Radar Requirements for DPCA Clutter Cancellation," Project Report SRT-27, Lincoln Laboratory, Massachusetts Institute of Technology, 27 November 1987.
5. E. J. Kelly, "Radar Surveillance from Space – System Concept and Radar Model," Project Report SRT-7, Lincoln Laboratory, Massachusetts Institute of Technology, 27 December 1983.
6. A. J. Fenn, F. G. Willwerth, and H. M. Aumann, "Displaced Phase Center Antenna Near-Field Measurements for Space-Based Radar Applications," Proceedings of the Phased Arrays 1985 Symposium, RADC-TR-85-171 In-House Report SRT-22, pp. 303-318, August 1985, ADA-169316.
7. H. M. Aumann, A. J. Fenn, and F. G. Willwerth, "A Self-Calibration and Pattern Prediction Technique for Phased Array Antennas," Project Report SRT-22, Lincoln Laboratory, Massachusetts Institute of Technology, 5 August 1986.
8. A. J. Fenn, "Phased Array Antenna Radiating Elements for a Space-Based Radar," Project Report SRT-4, Lincoln Laboratory, Massachusetts Institute of Technology, 8 September 1983.
9. A. J. Fenn, "Theoretical and Experimental Study of Monopole Phased Array Antennas," *IEEE Trans. Antennas Propag.*, Vol. AP-34, No. 10, pp.1118-1126, October 1985.
10. A. J. Fenn, "Monopole Phased Array Antenna Evaluation for a Low-Altitude Space-Based Radar." Project Report SRT-2, Lincoln Laboratory, Massachusetts Institute of Technology, 31 August 1983.
11. A. J. Fenn, "Element Gain Pattern Prediction for Finite Arrays of V-Dipole Antennas Over Ground Plane," *IEEE Trans. Antennas Propag.*, Vol. AP-36, No. 11, pp. 1629-1633, November 1988.

12. E. J. Kelly, "DPCA Implementation Issues," Space Radar Technology Program Review, 12-13 June 1985, Lincoln Laboratory, Massachusetts Institute of Technology.
13. R. C. Hansen, "Formulation of Echelon Dipole Mutual Impedance for Computer," *IEEE Trans. Antennas Propag.*, Vol. AP-20, No. 6, pp. 780-781, November 1972.
14. H. M. Aumann and F. G. Willwerth, "Design and Performance of a Very Low Sidelobe Phased Array Antenna," Project Report SRT-31, Lincoln Laboratory, Massachusetts Institute of Technology, 29 June 1988.
15. I. S. Reed, J. D. Mallet, and L. E. Brennan, "Rapid Convergence Rate in Adaptive Arrays," *IEEE Trans. Aerospace and Electronic Systems*, Vol. AES-10, No. 6, pp. 853-863, November 1974.
16. D. M. Boroson, "Sample Size Considerations for Adaptive Arrays," *IEEE Trans. Aerospace and Electronic Systems*, Vol. AES-16, No. 4, pp. 446-451, July 1980.

REPORT DOCUMENTATION PAGE			Form Approved OMB No. 0704-0188	
Public reporting burden for this collection of information is estimated to average 1 hour per response, including the time for reviewing instructions, searching existing data sources, gathering and maintaining the data needed, and completing and reviewing the collection of information. Send comments regarding this burden estimate or any other aspect of this collection of information, including suggestions for reducing this burden, to Washington Headquarters Services, Directorate for Information Operations and Reports, 1215 Jefferson Davis Highway, Suite 1204, Arlington, VA 22202-4302, and to the Office of Management and Budget, Paperwork Reduction Project (0704-0188), Washington, DC 20503.				
1. AGENCY USE ONLY (Leave blank)	2. REPORT DATE 5 September 2000	3. REPORT TYPE AND DATES COVERED Technical Report		
4. TITLE AND SUBTITLE Theoretical Effects of Array Mutual Coupling on Clutter Cancellation in Displaced Phase Center Antennas		5. FUNDING NUMBERS C - F19628-00-C-002		
6. AUTHOR(S) Alan J. Fenn and Edward J. Kelly				
7. PERFORMING ORGANIZATION NAME(S) AND ADDRESS(ES) Lincoln Laboratory, MIT 244 Wood Street Lexington, MA 02420-9108		8. PERFORMING ORGANIZATION REPORT NUMBER TR-1065		
9. SPONSORING/MONITORING AGENCY NAME(S) AND ADDRESS(ES) U.S. Air Force		10. SPONSORING/MONITORING AGENCY REPORT NUMBER ESC-TR-99-078		
11. SUPPLEMENTARY NOTES None				
12a. DISTRIBUTION/AVAILABILITY STATEMENT Approved for public release; distribution is unlimited.			12b. DISTRIBUTION CODE	
13. ABSTRACT (Maximum 200 words) This report has investigated the subject of array mutual coupling effects on the displaced phase center antenna clutter cancellation capability of corporate-fed phase array antennas. Mutual coupling effects have been modeled using the method of moments for monopole and dipole phased array antennas. Finite array edge effects and polarization are inherently included in the analysis. The assumption of an infinite ground plane was made in the theoretical formulation. The effect of transmit/receive module random errors have been ignored in this analysis. The theoretical results presented are the upper-bound clutter cancellation limited by mutual coupling alone.				
14. SUBJECT TERMS			15. NUMBER OF PAGES 68	
			16. PRICE CODE	
17. SECURITY CLASSIFICATION OF REPORT Unclassified	18. SECURITY CLASSIFICATION OF THIS PAGE Unclassified	19. SECURITY CLASSIFICATION OF ABSTRACT Unclassified	20. LIMITATION OF ABSTRACT Same as report	